Separation and Purification Technology 395 (2026) 137783

Contents lists available at ScienceDirect

Separation and Purification Technology

journal homepage: www.elsevier.com/locate/seppur

Rapid and sequential removal of polyphenols and heavy metals from water by zeolitic imidazolate framework-67 (ZIF-67)

Arvind Raj [a], Melissa G. Galloni [b,c], Ermelinda Falletta [b,c,*], Veronica Bortolotto [b], Nikoletta Mila [b], Giuseppina Cerrato [c,d], Valeria F.M. Mezzanotte [e], Mahaveer D. Kurkuri [a], Claudia L. Bianchi [b,c]

[a] Centre for Research in Functional Materials (CRFM), JAIN (Deemed-to-be University), Jain Global Campus, Bengaluru 562112, Karnataka, India
[b] Dipartimento di Chimica, Università Degli Studi di Milano, Via Golgi 19, 20133 Milano, Italy
[c] Consorzio Interuniversitario Nazionale per la Scienza e Tecnologia dei Materiali (INSTM), Via Giusti 9, 50121 Firenze, Italy
[d] Dipartimento di Chimica, Università degli Studi di Torino, Via Giuria 7, 10125 Torino, Italy
[e] Dipartimento di Scienze dell'Ambiente e della Terra, Università degli Studi di Milano Bicocca, Piazza della Scienza, 1, 20126, Milano, Italy

ARTICLE INFO

Keywords:
Metal-organic frameworks
Adsorption
Polyphenols
Heavy metals
Water remediation

ABSTRACT

Over the past decade, metal-organic frameworks (MOFs) have garnered significant scientific attention owing to their exceptional physicochemical properties and versatility across a wide range of applications. In this work, a circular economy strategy is adopted to address critical challenges associated with excessive waste generation, resource limitations, and economic sustainability. Specifically, the performance of the zeolitic imidazolate framework ZIF-67 was evaluated for the sequential removal of organic and inorganic contaminants from water. Pristine ZIF-67 was first employed for the adsorption of polyphenols, using gallic acid as a model compound, after which the spent material (ZIF@GA) was reutilised for the removal of heavy metal ions, including cadmium, lead, and chromium. ZIF-67 exhibited a maximum adsorption capacity of 171 mg/g for gallic acid, while ZIF@GA demonstrated an exceptionally high adsorption capacity of 1020 mg/g for Pb(II) ions, along with removal efficiencies of 58% and 45% for Cd(II) and Cr(VI), respectively under batch conditions. Rapid and quantitative adsorption of gallic acid was maintained even under complex water matrices. To overcome the practical limitations associated with dispersed MOF powders, a simple and rapid method was developed to fix ZIF-67 nanostructures directly onto conventional laboratory-grade filter sheets. Overall, these findings highlight the strong potential of ZIF-67 as a sustainable, efficient, and scalable material for advanced water remediation applications.

1. Introduction

Plants naturally contain an important class of chemicals, known as polyphenols [1], which are well-known for their antioxidant properties, leading to numerous potential health benefits, including improved heart health, blood sugar regulation, anti-inflammatory effects, and cancer prevention [2–5]. There are more than 8000 types of polyphenols found so far, which are mainly classified into four categories, namely flavonoids, polyphenolic amides, phenolic acids, and others [6]. When polyphenols are released into wastewater, as a result of food industry waste, agricultural waste, and plant waste, they represent a serious damage to the environment and to common water purification systems (biological treatments), as these compounds can harm aquatic life and disrupt ecosystems [7–10]. Moreover, when polyphenols are combined with other pollutants, like heavy metals and organic dyes, the toxic mixture can lead to serious environmental and public health issues [11,12]. Although many techniques have been developed for the polyphenols separation from water, such as chromatography [13], coagulation [14], membrane separation [15], preferential transport [16], and precipitation [17], their efficiency is limited, as well as scalability and cost. Among all the techniques covered above, adsorption is the most successful, as it is simple to process, affordable, scarcely sensitive to harmful substances, dependable, and extremely effective [18–20]. Furthermore, a wide range of materials are commonly employed as adsorbents, including graphene-based nanomaterials [21], activated carbon [22], nanofibers [23], sustainable carbon materials [24],

* Corresponding author at: Dipartimento di Chimica, Università Degli Studi di Milano, Via Golgi 19, 20133 Milano, Italy.
E-mail address: ermelinda.falletta@unimi.it (E. Falletta).

https://doi.org/10.1016/j.seppur.2026.137783
Received 3 January 2026; Received in revised form 14 March 2026; Accepted 27 March 2026
Available online 28 March 2026

agricultural waste [25], and nanoporous structures [26,27].

In this regard, it is well documented that Metal-Organic Frameworks (MOFs) are promising adsorbents and effective functional materials to regulate environmental pollution [28–32]. MOFs are hybrid crystalline structures that generate one-, two-, or three-dimensional porous frameworks by coordinating metal ions or clusters to organic ligands [33,34]. This class of porous materials has made rapid progress to the forefront of several materials research fields because of their remarkable properties. The utilization in water purification is associated to their notable features, like their very high surface areas, remarkable host-guest chemistry, chemically tuneable, and modular properties [35–37]. MOFs have a great deal of ability to adsorb organic contaminants, including organic dyes and pharmaceutical waste, and heavy metals from water [38,39]. However, polyphenols removal is still underinvestigated [40]. The structural versatility of MOFs makes them interesting, allowing for modifications aimed at increasing interactions with polyphenols and, therefore, increasing their adsorption capacity towards this class of compounds [41]. Interestingly, Bayazit et al. [42] used Zr-based MOF (UiO-66) for the removal of hydroxytyrosol and oleuropein from wastewater. Ghaedi et al. [43] investigated Cu-based MOF for the removal of gallic acid (GA) from orange juice samples. In particular, GA is a necessary polyphenol, utilised in medicine for its ability to reduce inflammation, allergies, mutagenesis reactions, and cancer [44]. Nevertheless, there are surprisingly few reports on the adsorption of polyphenols with MOFs.

Thanks to its structure and chemical composition, ZIF-67 emerges as a valid candidate for the adsorption of polyphenols. Cobalt ions, having a 2+ charge, tend to bind with the organic linker, i.e., 2-methylimidazole, forming a highly crystalline structure with a high surface area, making the material suitable for adsorption [45]. Furthermore, the synthesis of ZIF-67 is sustainable, simple, and facile, as the solvent used for the synthesis is either water or methanol, which makes ZIF-67 stand out from the other MOFs [46]. Besides, polyphenols, being negatively charged tend to adsorb on the surface of ZIF-67 due to their net positively charged structure. Although ZIF-67 is generally considered poorly water-stable, Qian et al. [47] have exposed undoped ZIF-67 for 10 days in water, and the structure slowly weakens and degrades after 10 days, as confirmed by XRD investigations. However, interestingly, Bendre et al. [48] adsorbed diclofenac sodium onto ZIF-67 for drug delivery application, wherein the diclofenac sodium loaded on ZIF-67 stayed for 6 days in aqueous media without leaching out the drug. This suggests that the intrinsic low stability of this material in aqueous media can be overcome by reducing the reaction time. Herein, ZIF-67 was first investigated as a promising adsorbent for the removal of polyphenols (in particular, GA) from different water matrices. Furthermore, the work implements the circular economy concept to address problems with limited resources, excessive waste production, and the preservation of economic gains [49]. In fact, while the adsorption process is an affordable means to clean water, it produces unwanted secondary waste as a result (spent adsorbent). In order to prevent the creation of additional waste [50], the ZIF-67 used for the removal of GA (ZIF-67@GA) was herein reutilised for the adsorption of heavy metals, such as Pb(II), Cd (II), and Cr(VI) with promising results. Thus, this study opens a new scope for the utilization of ZIF-67 for a multifunctional remediation approach.

2. Experimental section

The list of chemicals used, and the description of the characterisation techniques employed for the materials investigation are reported in the Supplementary Information file (S1 and S2, respectively).

2.1. Synthesis of ZIF-67

ZIF-67 was conventionally synthesised by sonicating 900 mg Co $(NO_3)_2.6H_2O$ and 1980 mg 2-MIM in 30 mL of methanol each. Both solutions were mixed in a beaker and continuously swirled with a magnetic stirrer (500 rpm) for 24 h (Fig. 1). The as-obtained precipitate was collected by centrifugation, methanol-washed, and dried at 80 °C overnight [48]. The material was obtained with a percentage yield of 84% and properly characterized, as described in the supplementary data (S2).

2.2. ZIF-67 water stability tests

To test the water stability of ZIF-67 a systematic stability study as a function of pH 3, 5, 9) and contact time (15 min and 24 h) was performed. Aqueous solutions buffered at pH 3, 5, and 9 were properly prepared by mixing the following solutions or buffer systems: nitric acid (0.5 M) acetic acid/sodium acetate, potassium di-hydrogen phosphate/di-sodium hydrogen phosphate, boric acid/potassium chloride/sodium hydroxide, sodium hydroxide (0.5 M). After immersion at selected pH values for predefined times, the solids were recovered, washed, and dried prior to characterisation. Structural integrity was evaluated by (i) FTIR spectroscopy to probe pore structure preservation and (ii) XRD to monitor crystalline phase retention. In addition, we monitored metal leaching in solution (Co concentration by ICP-OES).

2.3. Batch adsorption tests

Batch adsorption experiments were performed to investigate the adsorption capacity of ZIF-67 towards polyphenols (gallic acid (GA), 4-hydroxybenzoic acid (4-HB), Eudesmic acid (EA), caffeic acid (CA), trans-ferulic (t-FA)). The efficiency in GA abatement was also verified in the presence of organic dyes (methyl orange (MO), rhodamine (RB), methylene blue (MB), congo red (CR)), in the presence of salts ($NaNO_3$, NaCl, Na_2SO_4, $NaHCO_3$), and in the presence of humic acid (HA). Then, ZIF-67 loaded with GA was used for the removal of heavy metals, used as secondary pollutants (Pb(II), Cd(II), Cr(VI)).

2.3.1. Polyphenols adsorption tests

The tests were carried out in a 100 mL beaker maintaining a fixed adsorbent dosage (10 mg/L) and varying the GA concentration (10–1000 mg/L) of 20 mL of solution. The suspensions were magnetically stirred (500 rpm) at room temperature for 90 min. Finally, ZIF-67 was removed by centrifugation and the resulting solutions were analysed by UV–vis spectroscopy (Shimadzu, UV-2600) at $\lambda = 260$ nm. The gradual removal of polyphenols was monitored at different times. In addition, the effect of pH and ionic strength were investigated, varying the pH value and modifying the GA solution composition with the addition of different salts ($NaNO_3$, NaCl, Na_2SO_4) at a concentration of 0.05 M.

Eq. (1) was used to determine the removal efficiency in terms of percentage removal:

$$\%\text{Removal} = \frac{C0 - Cf}{Cf} * 100 \quad (1)$$

where "C_0" (mg/L) is the initial concentration of the target polyphenol and "Cf" (mg/L) is its final concentration.

Using Eq. (2), the adsorption capacity (qe) (mg/g) was calculated:

$$q_e = \frac{(C0 - Cf)\ V}{m} \quad (2)$$

where "C_0" (mg/L) is the initial concentration of the target polyphenol, "Cf" (mg/L) is its final concentration, "*V*" (L) and "m" (g) represent the solution volume and absorbent dosage, respectively.

2.3.2. Metals adsorption tests

ZIF-67 used for the removal of GA (now ZIF-67@GA) was subsequently tested for the removal of heavy metals (Pb(II), Cd(II), or Cr(VI)) as secondary pollutants. More in detail, 10 mg of ZIF-67@GA were

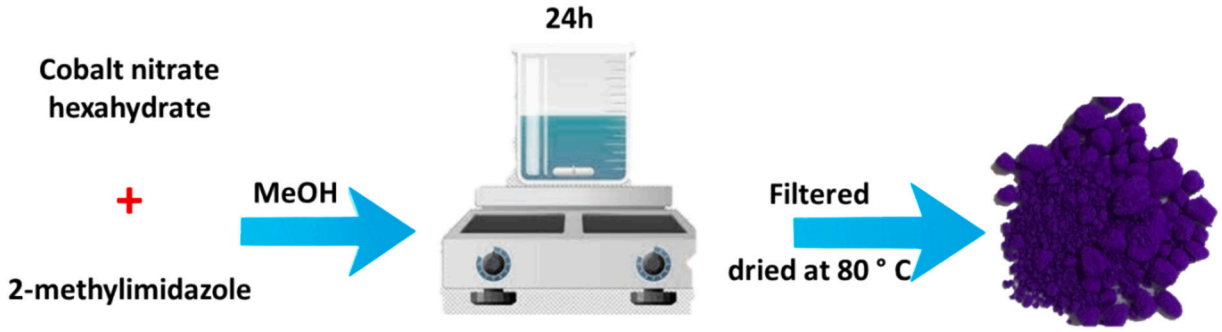

Fig. 1. Schematic representation of the synthesis of ZIF-67.

added to 10 mg/L metals solutions (20 mL). Each mixture was maintained under stirring for 15 min at room temperature. Aliquots were sampled, and the metal concentrations were verified by a PinAAcle 900 Series AA atomic absorption spectrometer equipped with a flame atomization system (Perkin Elmer) at $\lambda = 283.31$ nm, $\lambda = 228.80$ nm, and $\lambda = 357.87$ nm for Pb, Cd and Cr, respectively. The percentage of metal removal and adsorption capacity were determined by eqs. 1 and 2, respectively.

The adsorption capacity of ZIF@GA was also tested towards the removal of a mixture od heavy metals. More in detail, 10 mg of ZIF@GA were suspended in 20 mL of deionized water containing Pb(II), Cd(II), and Cr(VI). The concentration of each metal in solution was maintained at 3 mg/L.

2.3.3. Effect of water matrix

The selectivity of ZIF-67 towards GA removal was also studied in different conditions: i) in the presence of organic dyes (methyl orange, MO, rhodamine-B, RB, methylene blue, MB, congo red, CR), ii) using acidified tap water (to ensure GA stability), containing GA, humic acid (HA), and Pb(II) simultaneously. The presence of humic acid was intended to mimic natural organic matter, while the ionic background of tap water introduced additional inorganic species that may affect adsorption performance. For the tests in the presence of organic dyes, into 20 mL of 10 mg/L GA solutions, the dyes (single or as mixture) were added at a concentration of 10 mg/L. The organic species present in solution (both GA and organic dyes) were always in 1:1 mass ratio.

Then, ZIF-67 was added (adsorbent dosage 10 mg/L) and the suspensions were magnetically stirred (500 rpm) at room temperature for 30 min. Finally, ZIF-67 was removed by centrifugation and the resulting solutions were analysed by UV–vis spectroscopy. The chemical structure of the dyes and λ_{max} used for the adsorption investigations are shown in Table S1. Moreover, the effect of the presence of different salts ($NaNO_3$, NaCl, Na_2SO_4) on GA removal was also evaluated.

At first, in 20 mL of GA 10 mg/L solution the selected salt was added (0.05 M). Then, ZIF-67 was added (adsorbent dosage 10 mg/L), the suspensions were magnetically stirred (500 rpm) at room temperature. After 30 min, the mixture was treated with the same procedure reported above. The percentage of GA removal and adsorption capacity were determined by eqs. 1 and 2, respectively.

Concerning the tests in acidified tap water containing both GA and Pb(II), a simulated tap water matrix was prepared according to Annex B2 of the second protocol of the French Norm NF P41–650 [51], then acidified by a few drops of nitric acid (0.4 M) until 5 pH value was achieved. 2 mg of HA were added in 20 mL of the simulated tap water, followed by 2 mg of GA (GA concentration in the final solution = 100 mg/L). 10 mg of ZIF-67 were added, and the mixture was maintained under stirring. After 15 min, the adsorbent was removed by filtration and the variation in concentration of GA was monitored by UV–vis spectroscopy, and the percentage of GA removal and adsorption capacity were calculated as reported above.

2.3.4. Reusability tests

ZIF-67 was subjected to seven recycle tests. More in detail, 10 mg of ZIF-67 was suspended into 20 mL of 10 mg/L GA and magnetically stirred for 30 min. At the end of each run, the MOF was removed from the solution by centrifugation, washed with ethanol, dried and reused.

The removal efficiency of ZIF@GA towards Pb(II) was investigated over multiple adsorption cycles (five). At the end of each cycle, ZIF@GA was separated by centrifugation, washed with deionized water and reused.

2.4. Immobilisation of ZIF-67 on a filter paper and continuous flow-adsorption study

A ZIF-67 dispersion in deionized water (1 mg/mL; total volume = 30 mL) was filtered through a 55 mm diameter, 210 μm thick filter membrane support to create a homogeneous ZIF-67-based filter. More details are reported in the Supplementary Information file (S3). GA removal was performed on the ZIF-67-modified filter. 100 mL of GA solution (10 mg/L) was passed through the ZIF-67-modified filter in a continuous flow. The filtered solution was spectroscopically analysed, as reported above, and the percentage of GA removal and adsorption capacity were determined by eqs. 1 and 2, respectively.

3. Results and discussion

3.1. Characterisation

The successful obtaining of ZIF-67 was verified by several analytical techniques. Fig. 2 A compares the simulated pattern of ZIF-67 and the experimental pattern of the as-synthesised material. In addition, the CIF file of ZIF-67, stored in the Cambridge Crystallography database (CCDC-7247762), was used to realise the simulated pattern of ZIF-67 by Mercury 3.8 software. Furthermore, using the CIF file, the structure of ZIF-67 was realized using Vesta software (Fig. 2 B and C). The results demonstrate that the experimental XRD pattern was in good agreement with the simulated one. More in detail, the synthesised ZIF-67 displayed intense peaks at $2\theta = 7.5°$, 10.1°, and 12.8°, corresponding to (110), (200), and (211) planes, respectively. The absence of any extra signal confirms the purity of the obtained material.

The morphology and chemical composition of ZIF-67 were investigated by TEM, FESEM and EDX. Fig. 3 (A and B) exhibits individual particles of ZIF-67 with an average size in the 0.5–1.2 μm range. According to the literature [59,60], the predominant morphology of the particles is identified as chamfered cubes, specifically exhibiting a truncated rhombic dodecahedral structure, as also confirmed by the TEM results (Fig. 3H-*J*). The EDX mapping (Fig. 3C-G) identified and visualised the spatial distribution of the elements across the material's surface (56.4% C, 19.4% Co, 14.5% N, and 9.7% O), revealing a homogeneous composition. The presence of oxygen can be attributed to the water molecules present as a structural component in the MOF.

The functional groups of ZIF-67 were investigated by FTIR analysis,

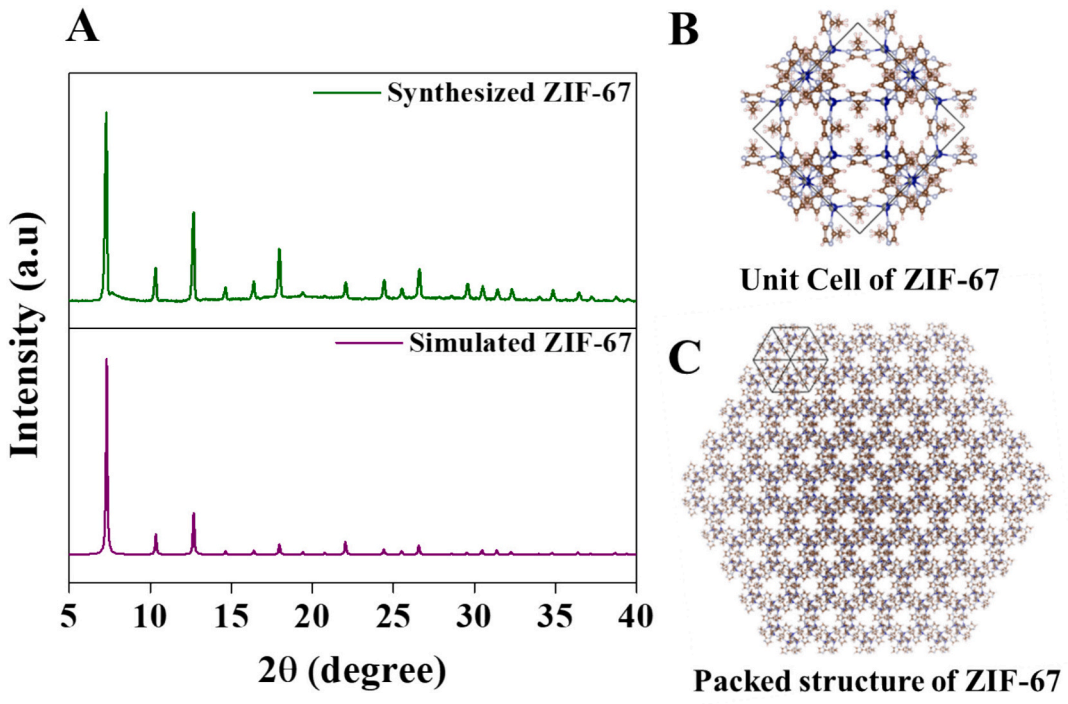

Fig. 2. A) Experimental (green) and simulated (purple) XRD patterns of ZIF-67; B) and C): unit cell and packed structure of ZIF-67, respectively. (For interpretation of the references to colour in this figure legend, the reader is referred to the web version of this article.)

as shown in Fig. 4 A. The bending vibration of the 2-methylimidazole ring may be responsible for the peak at 680 cm^{-1}. The peak at 756 cm^{-1} corresponds to the C—H bending of the linker, whereas the peak at 983 cm^{-1} is due to the occurrence of C—N bending vibration, and the stretching vibration of C—N is identified at 1141 cm^{-1}. Moreover, the vibrations of C═C and C═N bonds of the imidazole ring are responsible for the peaks at 1308 cm^{-1} and 1430 cm^{-1}, respectively. Beyond 2000 cm^{-1} no significant spectroscopic signals are present.

The thermal stability of ZIF-67 was verified by TGA analysis (Fig. 4 B). ZIF-67 exhibited an initial weight loss of 5% associated with the elimination of water molecules present on the MOF, in agreement with the TEM results. Interestingly, ZIF-67 was thermally stable up to 470 °C, whereas beyond this temperature, the framework collapses because of the decomposition of the organic linker (2-MIM), and the leftover 20% weight corresponds to the presence of cobalt ions, whose presence was confirmed by EDX analysis (Fig. 3C and D).

The N_2 adsorption-desorption isotherm of the synthesised MOF is shown in Fig. 4 C. ZIF-67 displayed a typical type II adsorption isotherm, with a type-4 hysteresis, which denotes a micro-mesoporous structure and slit-shaped pores. The Brunauer Emmett Teller (BET) surface area resulted in 1623 m^2/g. In addition, the mean pore diameter of ZIF-67 was 4.12 nm, in the range of mesopores (2–50 nm) (Fig. 4 D). The chemical composition of the ZIF-67 surface was determined by XPS investigations, and the results are reported in Fig. 5 A. The HR spectrum of C1s exhibited 2 peaks at 283.89 eV and 286.35 eV, corresponding to C═C and C═N, respectively (Fig. 5 B), wherein C═C and C═N correspond to the imidazole ring present in the organic linker (2-MIM). The HR spectrum of N1s (Fig. 5 C) exhibited 2 peaks at 397.25 eV and 400.65 eV, which correspond to pyrrolic N of the organic linker and Co—N bond between the metal and ligand, respectively. The HR spectrum of Co 2p (Fig. 5 D) exhibited 2 peaks at 790.16 eV and 793.78 eV, attributed to Co $2p_{3/2}$ and Co $2p_{1/2}$, respectively, wherein Co $2p_{3/2}$ corresponds to the +3-oxidation state of Co, and Co $2p_{1/2}$ corresponds to the +2-oxidation state of Co. Furthermore, the peak in the survey spectrum for oxygen at 535 eV with a single broad peak can be attributed to adsorbed oxygen, surface lattice oxygen, as well as adsorbed water (Fig. S1).

If on one hand, the thermal stability of ZIF-67 is well documented and demonstrated [52], on the other hand, its water stability is controversial. In fact, some authors demonstrate that ZIF-67 is not stable in an aqueous environment owing to the spontaneous hydrolysis of ZIF-67 due to the breaking of the weak Co-Imidazolate bond [53], whereas others demonstrate their outstanding performances in water treatment [54–56]. The ZIF-67 water stability is a function of exposure time, as its framework's cobalt-nitrogen bonds are susceptible to hydrolysis, causing structural degradation, especially in prolonged aqueous conditions [47]. Fig. 6 displays the XRD results of the water stability test over time for the as synthesised ZIF-67.

As it is possible to observe, after 2.5 h of water exposure, the framework of the synthesised ZIF-67 began to collapse, according to the literature. However, thanks to the extremely fast adsorption kinetics of ZIF-67 towards organic species (as reported below), this did not represent a limit for the present application. Therefore, ZIF-67 is best suited for rapid or single-pass adsorption processes rather than prolonged batch treatments. Similarly, stability tests at different pH values were performed, because they are an important aspect for materials' characterisation. However, as for the water stability studies, also in this case the results of the various characterisation studies of any material should be functional to its practical application. In this regard, it is worth noting that polyphenols are generally unstable in alkaline conditions, degrading, oxidising, and dimerising more readily as pH increases (e.g., above 7), whereas in acidic environments they provide greater stability [57].

However, the ZIF-67 stability is also a function of the pH value of the water matrices where it is suspended and the exposure time, as its framework's cobalt-nitrogen bonds are susceptible to hydrolysis, causing structural degradation, especially in acidic media [47]. In fact, in severe acidic conditions, ZIF-67 degrades quickly because the methylimidazole linkers get protonated, weakening the Co—N coordination bonds, leading to framework collapse.

Therefore, any attempt to treat ZIF-67 at acidic (≤ 3) or alkaline (≥ 10) pH values failed, resulting in complete degradation of the material even for short exposure times.

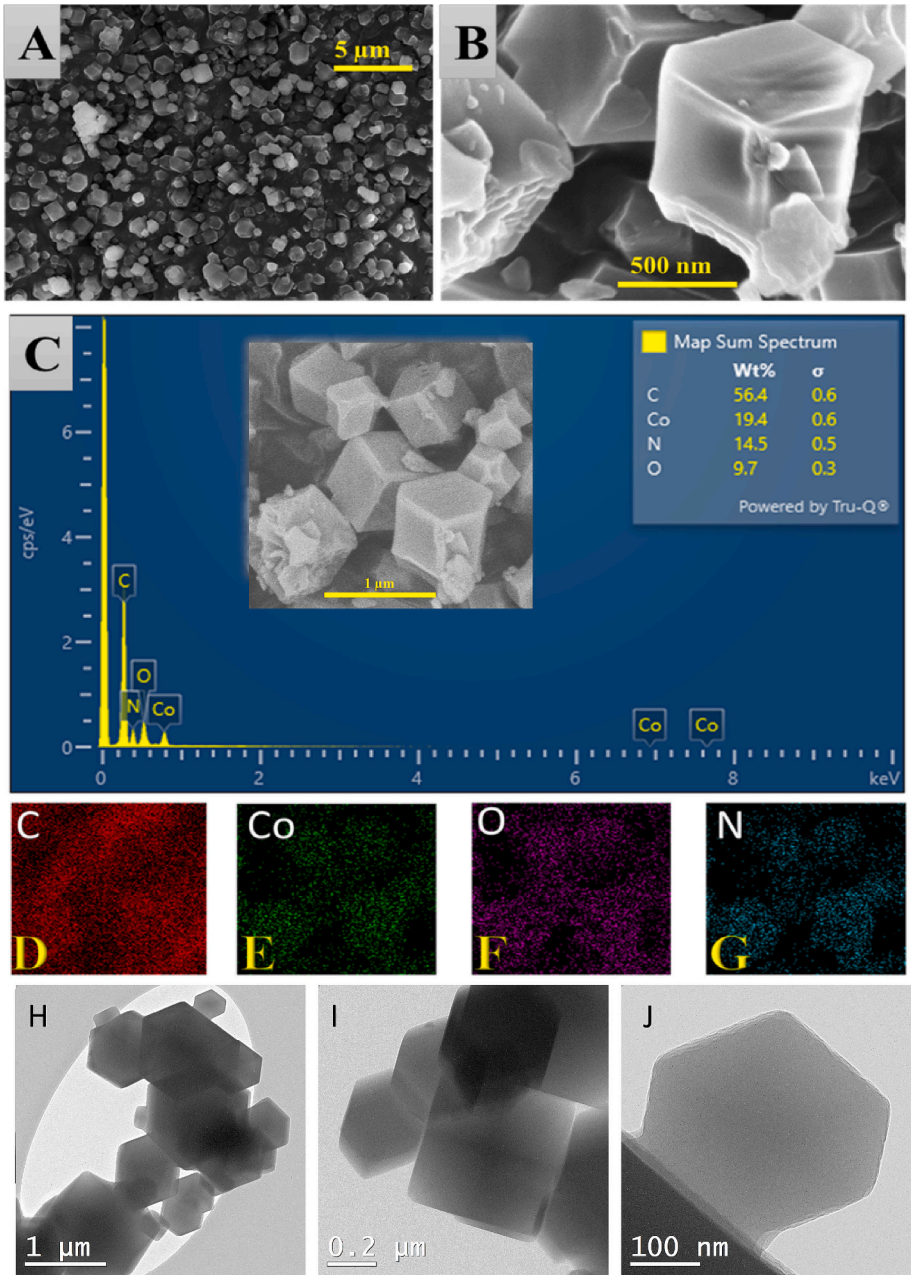

Fig. 3. A and B) FESEM images; C) EDX spectrum; D-G) elemental mapping; H-J) TEM images of ZIF-67.

In contrast, when exposed to aqueous solutions buffered at pH 3–9, the synthesised material maintained a certain stability for short exposure time, which then decreased over longer periods (24 h) (Fig. S2). Fig. S2 presents the FTIR spectra of ZIF-67 and ZIF@GA following treatment in different aqueous environments (pH 3, 5 (spontaneous pH), and 9) for 15 min and 24 h. For a short exposure time (15 min), the FTIR spectra of both ZIF-67 and ZIF@GA (Fig. S2 A and C) show only minor changes compared to the pristine MOF. All the characteristic bands remain present, with no significant variations in intensity.

Specifically, the band at 427 cm^{-1} is assigned to the Co—N stretching vibration. The peaks at 2924 cm^{-1} and 1578 cm^{-1} correspond to the C—H stretching vibration of the methyl group and the C═N stretching vibration of the imidazole ring, respectively. The broad band observed at 3425 cm^{-1} is attributed to hydroxyl groups from physically adsorbed water. The stretching vibration within the imidazole ring appears at 1416 cm^{-1}. Finally, the bands in the range 1168–1146 cm^{-1} are related to out-of-plane bending vibrations, while the signal at 992 cm^{-1} is associated with in-plane bending vibrations.

In contrast, after prolonged exposure (24 h) to both acidic and alkaline environments (pH 3 and 9), for ZIF-67 noticeable changes are observed (Fig. S2 B), including variations in peak intensities, appearance of new peaks at 3447 cm^{-1} is because the OH-stretching vibration of the surface hydroxyl groups, which are formed as a result of the interaction of the water molecules with the coordinatively unsaturated metal sites. Moreover, the broad peak in the 1650–1350 cm^{-1} spectrum could be explained by the bending vibration of the adsorbed water molecules, which was related to the broad O—H stretching band at a wavenumber of about 3450 cm^{-1}. Furthermore, the disappearance of the band at 427 cm^{-1} assigned to the Co—N stretching vibration, indicating chemical alterations.

The structure change is more pronounced in the FTIR spectra of ZIF@GA (Fig. S2 D) where the broadening of peaks in the ranges 1386–1568 cm^{-1} suggests structural deformation of the imidazole ring [58]. Also, the peak at 3434 cm^{-1} corresponds to OH^- stretching

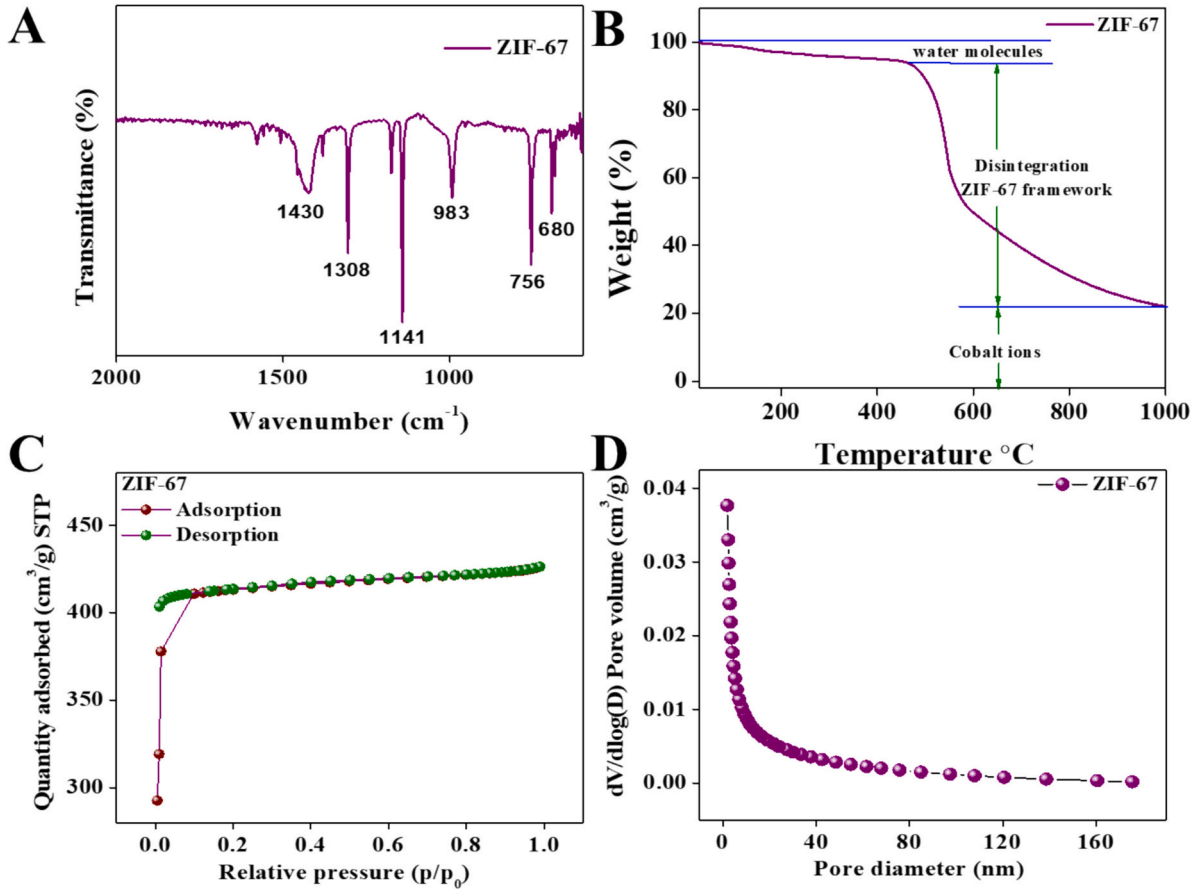

Fig. 4. A) FTIR spectrum; B) TGA spectrum; C) N_2 adsorption/desorption isotherm; D) Mean pore diameter of ZIF-67.

vibration.

According to the FTIR investigations, the crystallinity studies (Fig. S2 *E*-H) revealed a complete perturbation of the crystal structure only after prolonged water exposure (24 h) (Fig. S2 F and H), whereas the XRD signals remain unchanged for short water treatment (15 min) (Fig. S2 E and G).

The aqueous solutions used for each of these tests were analysed by the ICP-OES technique to quantify potential Co leaching due to ZIF-67 and ZIF@GA degradation. As reported in the literature [47], the framework of ZIF-67 cobalt-nitrogen bonds is susceptible to hydrolysis, causing structural degradation, especially in acidic media. The results (Table S2) demonstrated very low cobalt leaching for both materials under the different environmental conditions.

As expected, in acidic conditions and for long exposure time, the leaching is more pronounced.

Moreover, the percentage of cobalt release is one order of magnitude greater for ZIF@GA compared to ZIF-67. This different behavior can be attributed to a certain instability of ZIF-67 structure when exposed to GA, probably associated with a partial substitution of the organic linker (2-MIM) with GA.

The bioluminescence test was chosen to investigate the possible toxicity of the effluent of ZIP-67 treatment. The test is recognized at international scale as a useful tool for the ecotoxicological monitoring of water and solid samples. The target organism is a bioluminescent bacterium (*Aliivibrio fischeri*) and the acute toxicity is measured as a decrease of the bioluminescence emitted after 5 and 15 min of exposure. The bioluminescence test was performed on the effluent derived by the suspension of ZIF-67 for 15 min in deionized water at spontaneous pH (5). The 81.9% Basic Test protocol was applied, including a blank control and serial dilutions of the sample, and the luminescence signal was measured after 5, 15, and 30 min of exposure (Table S3). The results showed that bioluminescence emission increases with time also in the blanks and does not decrease with increasing concentrations of the sample. No concentration-dependent inhibition of bioluminescence emission occurred.

Therefore, the sample shows no evidence of appreciable acute toxicity under the tested conditions.

3.2. *Effect of contact time, temperature and initial concentration on GA adsorption*

Quick adsorption kinetics is crucial for adsorption processes. In particular, as reported above, this is a crucial point for ZIF-67 that suffers from being exposed to aqueous environments for prolonged periods, because of the spontaneous hydrolysis of ZIF-67, due to breaking of the weak Co-Imidazolate bond [53]. Fig. 7 depicts the effect of contact time on the GA abatement at different initial concentrations in the range 10–1000 mg/L.

As it is possible to observe, at low to moderate GA concentrations (10–100 mg/L), the polyphenol was rapidly and effectively adsorbed on the active sites of the synthesised MOF, which remain fully available under these conditions. In contrast, at higher initial GA concentration (1000 mg/L) the uptake rose sharply in the first minutes of the experiment, confirming a fast adsorption rate, but subsequently levels off as equilibrium approaches. This plateau confirmed that the adsorbent reached its saturation capacity. In these conditions, after 30 min treatment, ZIF-67 was able to absorb 39% of the initial GA amount.

Although the scientific literature reports several works on the adsorbent capacities of ZIF-67 towards phenols [59,60], it lacks studies on polyphenol removal. Moreover, to be useful and effective in real conditions, an adsorbent material should be able to remove a good part of polyphenols that are generally present in wastewater in

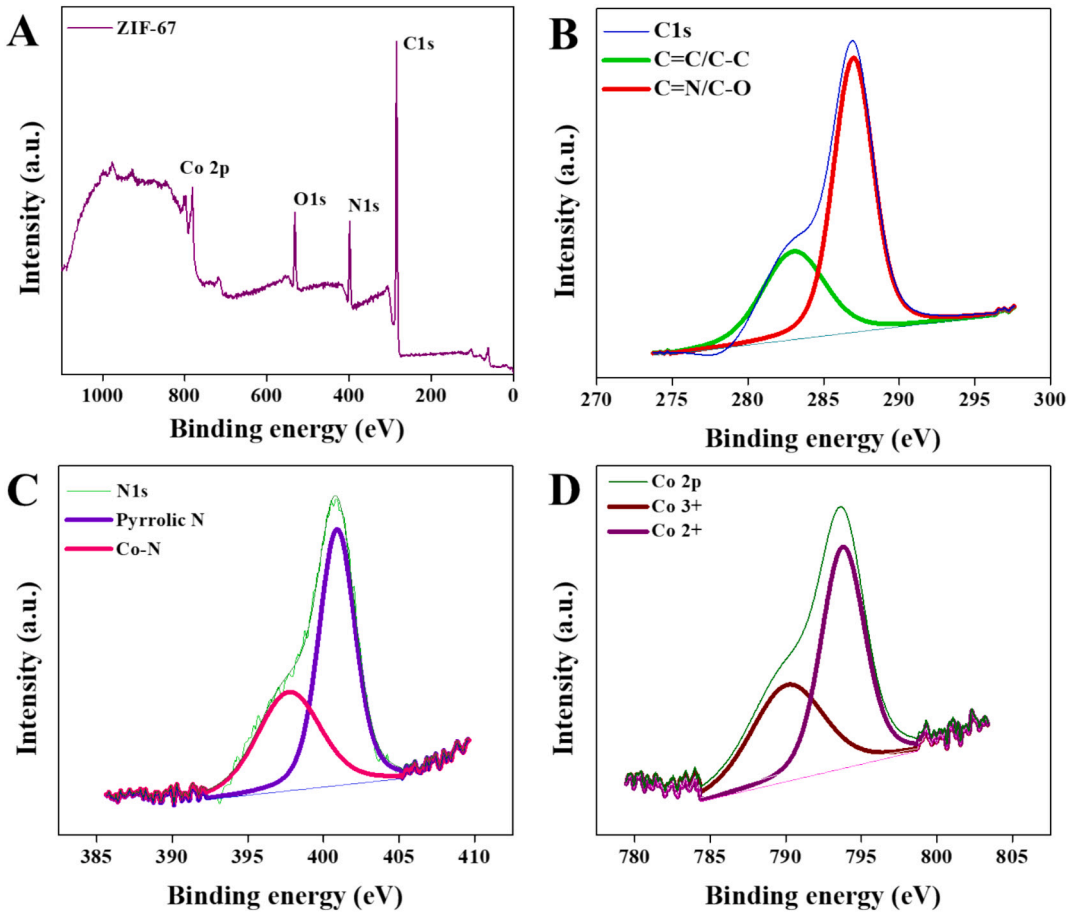

Fig. 5. A) XPS survey spectrum; B—D) High-resolution spectra of C1s, N1s, and Co2p, respectively, of ZIF-67.

concentrations of 0,1–20 g/L. In this scenario, ZIF-67 stands out as a promising candidate, removing from 100% to 39% of GA for an initial polyphenol concentration of 0.1–1 g/L. Fig. S3 displays the adsorption capacity of ZIF-67 towards GA at different temperatures. It is worth to notice that temperature variation did not have a significant impact on the material's performance. This behavior can be attributed to the minimal influence of temperature variation on the intermolecular electrostatic interactions governing the adsorption process.

ZIF-67 used for GA adsorption (ZIF@GA) was characterized in depth by several techniques (XRD, BET, XPS, and FTIR) to assess its stability, and the results are summarised in the Supporting Information (Fig. S4). The XRD pattern of the spent material (Fig. S4 A) confirms that the ZIF-67 retained its structure even after GA adsorption. The N_2 adsorption/desorption isotherm of ZIF-67@GA was still of type II (Fig. S4 B) with a strongly reduced value of surface area (78.50 m^2/g). The decrease in surface area, compared to the pristine material (1623 m^2/g), was due to the loading of GA onto the framework of ZIF-67, which partially blocked the pores and consequently reduced the accessible porous structure. Furthermore, ZIF@GA exhibited a type-4 hysteresis indicative of micro-mesoporous structure, with a mean pore diameter of 15.18 nm (Fig. S4 C).

As shown in Fig. S4 D, the FT-IR spectra of pristine ZIF-67 and ZIF@GA exhibit important differences. More in detail, the FTIR spectrum of GA is characterized by the stretching bands of C═O and C═C at 1675 cm^{-1} and 1540 cm^{-1}, respectively, due to the presence of a protonated carboxylic acid group and aromatic ring. On other hand, ZIF@GA exhibits two characteristic signals at 1380 cm^{-1} and 1565 cm^{-1}, associated to the presence of the symmetric and asymmetric stretching vibrations of the carboxylate group of gallate-metal species [61]. These results confirm the formation of gallate-Co species on the surface of ZIF-67.

The changes in the chemical states and the bonding environment of the elements after the adsorption of GA were analysed through XPS analysis. The ZIF@GA survey spectrum (Fig. S5 A) showed that all elements, including Co, O, and C, were retained except for N, suggesting that GA covers N reducing the intensity of its signal. The HR spectrum of C1s is deconvolutes in 2 peaks at 281.34 eV and 283.35 eV, corresponding to C—C and C═O, respectively (Fig. S5 B), associated to GA. Similarly, the HR spectrum of O1s (Fig. S5 D) can be deconvoluted in 3 peaks at 532.24 eV, 530.13 eV and 526.39 eV corresponding to the O-C═O, OH and Co—O, respectively, wherein the O-C═O and OH are from the carboxyl group of GA. The HR spectrum of Co 2p (Fig. S5 C) exhibited 2 peaks at 783.76 eV and 801.78 eV, which correspond to Co $2p_{3/2}$ and Co $2p_{1/2}$, respectively, wherein Co $2p_{3/2}$ corresponds to the +3 oxidation state of Co, and Co $2p_{1/2}$ corresponds to the +2 oxidation state of Co as the N from the imidazole ring binds with the Co ion.

As reported above for FTIR investigation, during GA adsorption, the formation of Co(II)-gallate complexes with possible cyclic Co(II)/Co(III) redox in the presence of O_2 cannot be ruled out. The clear colour change of ZIF-67 observed after adsorption tests (pristine ZIF-67 purple → used ZIF-67 darker shade (Fig. 12 below)) water molecules coordinating with Co^{2+} and altering its ligand field environment. In the high-resolution Co 2p XPS spectrum of the used material (Fig. S5 C), the intensity increase of the Co(III) peak confirms the previous hypothesis.

3.2.1. *Effects of salts and organic interferences on GA adsorption*

Numerous metal ions and salts present in industrial wastewater might act as interfering agents in the adsorption processes. Their presence may compete with or disrupt the interaction between the adsorbent and the target species. The influence of salts on the adsorption

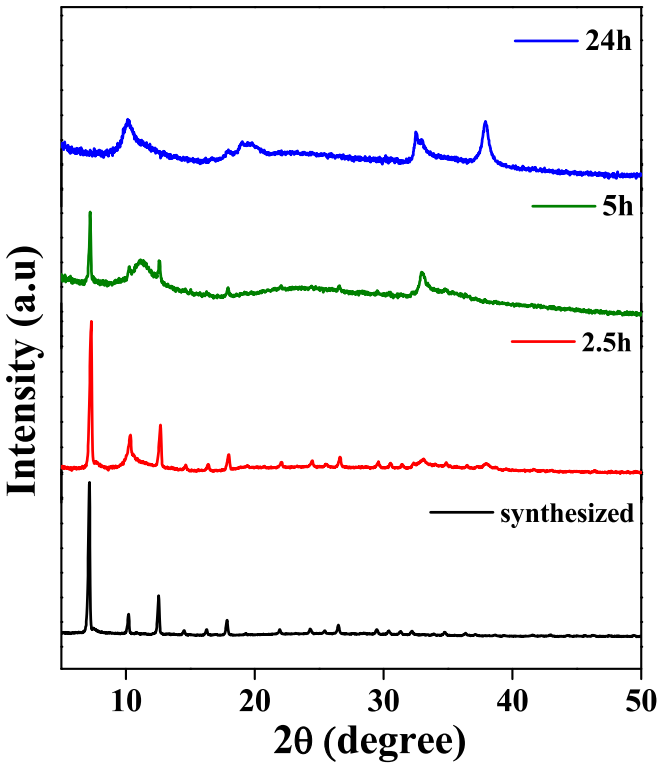

Fig. 6. XRD patterns of the synthesised ZIF-67, after 2.5, 5, and 24 h of water exposure.

performances of ZIF-67 towards GA adsorption was properly investigated by adding different sodium salts, including nitrate, sulphate, and chloride.

Fig. 8 A displays that ZIF-67 maintains excellent removal efficiency towards GA removal even in the presence of sodium salts, with values exceeding 95%. Bicarbonate salts were not investigated as potential interferences because of the low stability of both polyphenols and ZIF-67 in alkaline conditions, as discussed above.

The adsorption performance of ZIF-67 towards GA was also assessed in the presence of organic dyes. The effect of both anionic (CR and MO) and cationic dyes (MB and RB), evaluated either as single components or in combinations, anionic (MO + CR), cationic (MB + RB), and mixed anionic-cationic (CR + MB), was investigated, and the results are shown in Fig. 8 B and Fig. S6. The molecular structure and the absorption maximum wavelength of the selected dyes are displayed in Table S1. The results indicate that ZIF-67 maintained a high GA removal efficiency in the presence of anionic dyes and their mixtures, although a slight decrease was recorded moving from CR to MO. In contrast, the simultaneous presence of cationic dyes led to a noticeable deterioration of the ZIF-67 performance. Previous investigations on dye removal by ZIF-67 have demonstrated the promising activity of this material for the removal from water matrices, particularly for anionic dyes by π-π stacking interactions and coordination between the nitrogen and oxygen atoms of dye molecules and the metal ions in the ZIF-67 [62,63]. Based on these considerations, although anionic dyes can compete with GA for the active sites of the adsorbent, it is possible to conclude that they can simultaneously act as a secondary adsorption shell surrounding the ZIF-67 particles. This effect likely enhances GA uptake by promoting interactions between the amino groups on the aromatic rings of CR and MO and the carboxylic group of GA. In contrast, although cationic dyes were partially adsorbed on ZIF-67, their positive charges can cause electrostatic repulsion, hindering GA adsorption and reducing the overall efficiency.

3.2.2. *Selectivity investigation*

The selectivity of ZIF-67 towards the removal of other polyphenols, such as caffeic acid (CA), trans-ferulic acid (t-FA), 4-hydroxybenzoic acid (4-HBA), and eudesmic acid (EA), in addition to GA, was also investigated, and the results are reported in Fig. 9.

The comparison of the 100% removal efficiency achieved for GA with the efficiencies measured for the other polyphenols reveals the following decreasing trend: GA = CA > 4-HBA > t-FA > EA. By examining the results reported in Fig. 9 with the chemical structure of the selected polyphenols (Fig. S7), it is evident that the ZIF-67 removal capacity is influenced by the number of hydroxy groups (-OH) on the benzene ring of the investigated compounds.

GA has three hydroxyl groups on the benzene ring, whereas CA contains only two.

However, in both cases the hydroxyl groups are arranged in a vicinal (adjacent) position, permitting strong coordination interactions with the Co(II) centres of the ZIF-67, and consequently promoting high removal efficiency. In contrast, 4-HBA and t-FA possess only a single hydroxyl group on the benzene ring. Although ZIF-67 still removed a certain fraction of these compounds, the performances were markedly lower, because the single OH group interacts less with the Co(II) sites. The reduced removal efficiency observed for t-FA can be attributed to the presence of the adjacent -OCH_3 group, causing steric hindrance and further weakening its interaction with the adsorbent. Finally, the absence of any hydroxyl group in the chemical structure of EA accounts

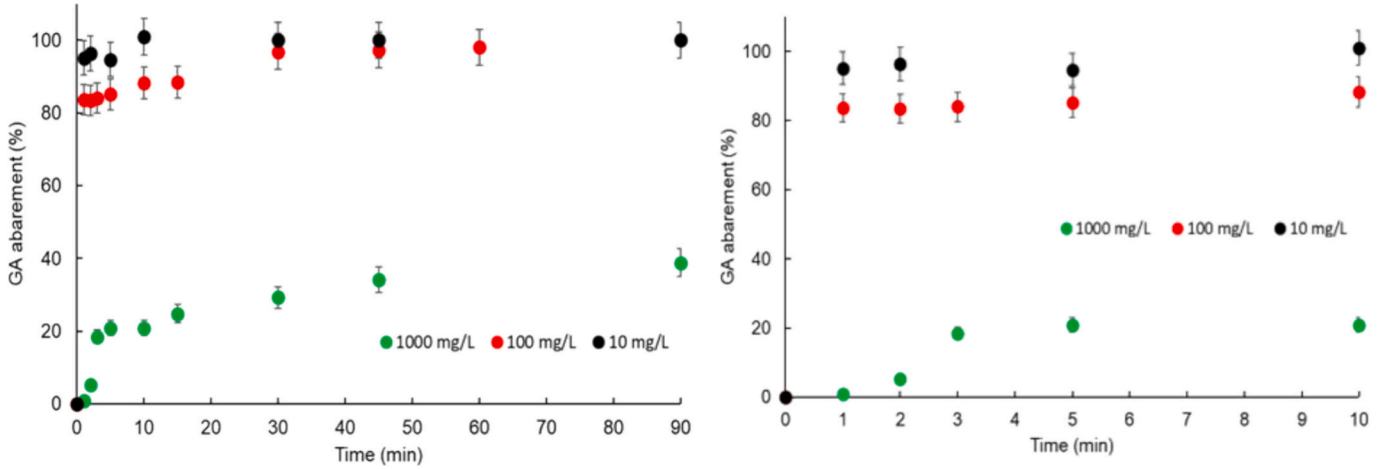

Fig. 7. Adsorption uptake with time at different initial GA concentrations (C_{GA} = 10 mg/L, 100 mg/L, 1000 mg/L). In the inset, an expansion in the time window 0–10 min is reported.

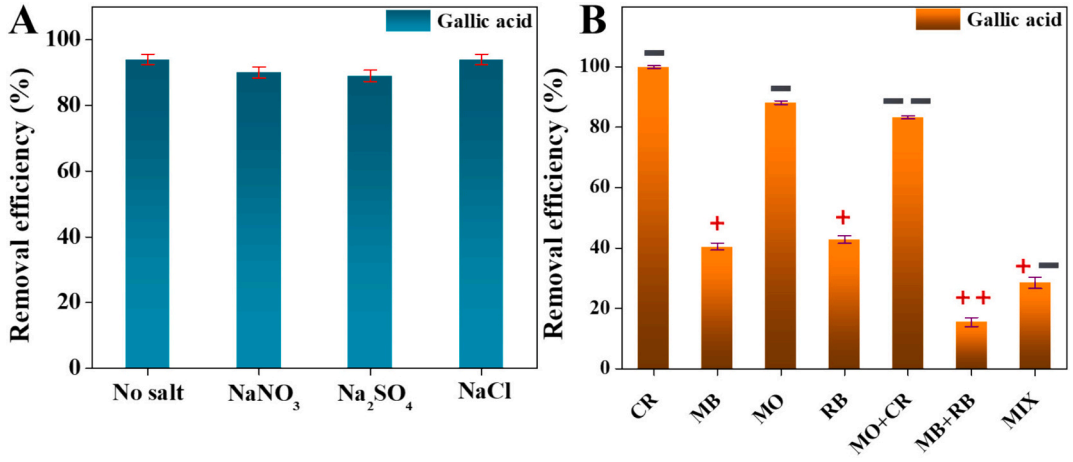

Fig. 8. A) Percentage of GA removal by ZIF-67 in the presence of: A) sodium salts, B) organic dyes. Initial C_{GA} = 10 mg/L, Initial C_{dye} = 10 mg/L.

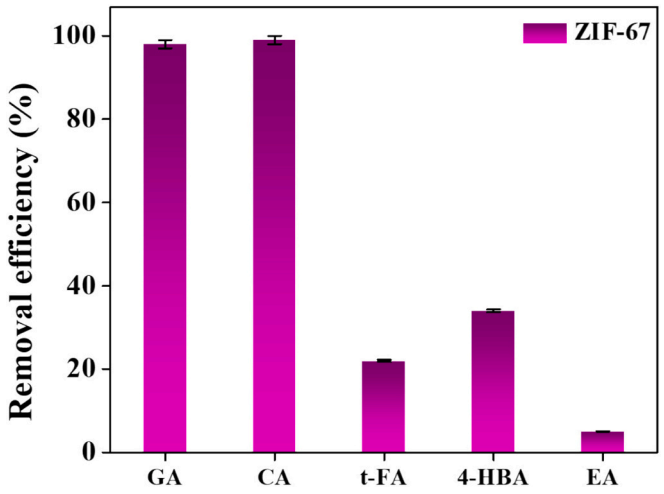

Fig. 9. Percentage of polyphenols removal using ZIF-67. Initial concentration of polyphenols = 10 mg/L.

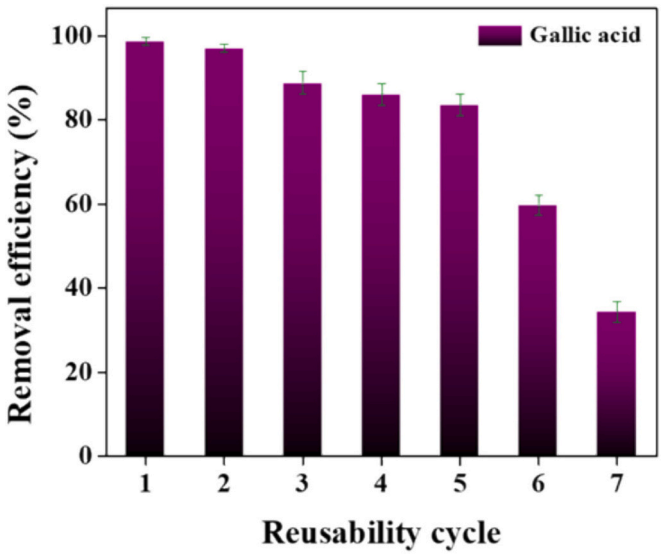

Fig. 10. Reusability test of ZIF-67 for GA removal over 7 consecutive cycles: initial C_{GA} = 10 mg/L.

for its poor adsorption. Concluding, ZIF-67 is a promising adsorbent for polyphenols characterized by the presence of hydroxyl groups on the benzene ring, whereas its effectiveness markedly decreases for molecules lacking such functional groups.

3.2.3. *Reusability*

To assess the stability of ZIF-67 under the reaction conditions, a reusability test was performed for up to seven adsorption-desorption cycles. As shown in Fig. 10, ZIF-67 retained a removal efficiency above 95% during the first two cycles, and relatively stable performance up to the fifth cycle. However, a pronounced decline in adsorption efficiency was observed during the sixth and seventh cycles. This deterioration can be reasonably attributed to cumulative pore blockage by residual adsorbate species, partial occupation of active coordination sites, and gradual structural destabilization during repeated adsorption-desorption treatments [64]. These effects collectively reduce accessible surface area and hinder mass transfer, ultimately leading to diminished adsorption performance beyond the stable regeneration limit.

Nevertheless, the adsorbed polyphenols can be readily recovered by washing the material with ethanol, followed by evaporation of the solvent. To evaluate the structural evolution of the materials after repeated GA adsorption-desorption cycles, FTIR, XRD, and BET analyses were performed, and the results are reported as shown in Fig. S8.

The FTIR spectrum (Fig. S8 A) of the spent MOF displays the characteristic Co—N stretching band (528 cm^{-1}) of ZIF-67. However, the other characteristic functional groups of the MOF are not clearly visible, as after seven cycles the framework is covered with GA. The bands at 1506 cm^{-1} and 1361 cm^{-1} refer to symmetric and asymmetric stretching vibrations of the carboxylic O-C=O bond of GAs, as well as the broad signal at 3412 cm^{-1}, associated with the OH stretching of GA. The major diffraction peaks of spent ZIF-67 are preserved, as shown in Fig. S8 B, confirming retention of the crystalline framework. Nevertheless, there are shifts in minor peaks and new peaks, associated with pore blockage and GA adsorption.

Finally, a noticeable decrease in the specific surface area (< 1 m^2/g (0.75 m^2/g)) and mean pore diameter (to 3 nm) was observed after repeated cycles by BET analysis (Fig. S8 C). Also, this reduction is primarily attributed to partial pore blockage by residual GA molecules and slight framework destabilization during regeneration. The diminished porosity directly limits the accessibility of active sites, which correlates well with the pronounced decline in adsorption capacity observed beyond the seventh cycle.

3.3. *Adsorption kinetics*

To investigate the adsorption kinetics of ZIF-67 towards GA, both the

pseudo-first order (PFO) and the pseudo-second order (PSO) reaction models were used. These models were fitted to the experimental data to evaluate the rate mechanisms governing the adsorption process, using the linearized forms presented in eq. S1 and S2. The resulting kinetic parameters are summarised in Table 1. Figs. S9 A and B display the kinetic model plots for the adsorption of GA onto ZIF-67. The PSO model displayed a superior fit compared to PFO, as resulted by the R^2 value closer to 1. Additionally, the agreement between the estimated values and the experimental one support the suitability of the PSO model in describing the adsorption kinetics of GA on ZIF-67.

Using the Weber-Morris equation (eq. S3), the diffusion mechanisms governing the adsorption process were investigated. This model allows the estimation of the contribution of the intra-particle diffusion to the adsorption rate. For ZIF-67, the regression plot shows a linear region that does not pass through the origin (Fig. S9 C), suggesting that the intra-particle diffusion is not the unique process responsible of the rate-controlling. The boundary layer diffusion or external mass transfer plays a crucial role, as reflected by the intercept value (C = 0.0471).

However, as the previous observed, both surface diffusion and intra-particle diffusion significantly influence the adsorption mechanism. To further determine which step primarily controls the adsorption rate of adsorption and to clarify which factor has a greater impact, the Boyd kinetic model was applied. By eq. S4 a plot "Bt" vs. time "t" yields the Boyd plot (Fig. S9 D), characterized by a straight line that does not pass through the origin. This indicated that surface diffusion is the primary rate-controlling step. This finding corroborates the results of the Weber–Morris analysis, confirming that surface diffusion or film diffusion mostly determine the adsorption kinetic of GA onto ZIF-67.

3.3.1. Adsorption isotherm

Adsorption isotherms investigations were carried out for the GA removal by ZIF-67, and the corresponding parameters are reported in Table 2, whereas the fitted isotherm plots are shown in Fig. S10 A and B. Widely accepted isotherm models, like Langmuir and Freundlich, were employed to simulate the experimental data in order to study the nature and progress of the adsorption process (eq. S5-S7). The Langmuir isotherm assumes monolayer adsorption on a homogeneous surface with uniformly energy-dense, finite, and defined active sites. Conversely, the Freundlich model accounts for multilayer adsorption on heterogeneous surfaces possessing sites with varying adsorption energies [65]. Based on the results displayed in Fig. S10 A and B, the Freundlich isotherm seems to display a superior fit compared to the Langmuir isotherm with an R^2 value closer to 1. This suggests that the adsorption of GA onto ZIF-67 is better described by a multilayer adsorption mechanism occurring on heterogeneous surface sites.

Furthermore, the concentration of the substance is crucial in determining the adsorption performance of a material. Based on the concentration study and using eqs. 1 and 2, it was observed that when 10 mg of MOF was employed, removal efficiency exceeding 99% were achieved for GA concentrations up to 20 mg/L. However, as the initial GA concentration increased, the adsorption efficiency gradually declined due to the progressive saturation of the active sites.

3.3.2. Adsorption mechanism

The plausible mechanism for the adsorption of GA could be associated with multiple synergistic interactions between the MOF and the polyphenol molecule (Fig. 11). The positively charged metal centres on the ZIF-67 surface can engage in electrostatic interactions with the functional groups of GA (hydroxyl and carboxyl groups). The XPS results revealed that cobalt ions in ZIF-67 exist in both +2 and + 3 oxidation states, enabling different modes of interaction according to the Hard Acid Soft Base (HSAB) principle [66], or promoting coordination interactions. Both oxidation states can coordinate with the hydroxyl functionalities of GA, leading to the formation of stable metal–ligand complexes. These coordination interactions, combined with electrostatic attraction and other surface forces, contribute significantly to the adsorption of GA onto ZIF-67.

Table 2
Outline of Langmuir and Freundlich isotherm parameters for ZIF-67.

Langmuir isotherm			Freundlich isotherm		
K_L (L/mg)	R_L	R^2	1/n	K_F	R^2
31.20	0.00318	0.4532	2.5109	8.07476	0.92167

3.4. Continuous flow adsorption study

The use of adsorbents in powder form presents several practical challenges, such as difficult separation from liquids, handling issues, high pressure drops when used in packed beds systems, etc. These limitations are mainly associated with their fine particle size, which makes recovery challenging, and to the potential loss of surface area during repeated use, necessitating efficient regeneration strategies. Although many approaches have been investigated to overcome these drawbacks (immobilisation in membranes, foams, beads, and natural materials, preparation of magnetically modified MOFs, etc. [67]), the simplest and cheapest method remains the adsorbent immobilisation of adsorbents on commercial filter paper. Zr-based MOF have been successfully immobilised on carboxymethylated filter paper for the removal of methylene blue from water [68]. Similarly, Yang et al. reported the fabrication of NH_2-MIL-125 (Ti)-modified filter paper for the removal of organophosphorus pesticides from aqueous solution and vegetables [69], to name a few.

Some studies have already been already reported to support ZIFs on paper filters. Cai et al. successfully loaded ZIF-67 on a commercial paper filter to fabricate a catalytic filter paper for the degradation of bisphenol A in water by peroxymonosulfate activation [70]. Abdelhamid and Mathew proposed Whatman® cellulosic filter paper as a support for both ZIF-8 and ZIF-67 for the catalytic reduction of 4-nitrophenol [71]. Additionally, Park and Oh investigated the adsorption performance of both ZIF-8 and ZIF-67 grown on carboxymethylated cellulose filter paper towards anionic dyes [72].

These studies collectively highlight the versatility and potential of paper-supported ZIF materials for catalytic and adsorption applications.

Here, a ZIF-67-modified filter paper was tested for the continuous-flow removal of GA, as shown in *V*ideo 1 and Fig. 12 A. At the beginning, the adsorption performance of the pristine (unmodified) filter membrane towards GA was evaluated under identical experimental conditions. The results (Fig. S11) showed negligible GA removal. Then, an aqueous ZIF-67 dispersion (1 mg/mL in 30 mL of deionized water) was filtered through a Whatman filter paper support to fabricate a ZIF-67-based filter. The modified filter paper was mounted in a dead-end filtration setup, and 100 mL of GA solution (10 mg/L) was prepared

Table 1
Kinetic parameters obtained from the PSO and PSO, and Weber-Morris models for GA adsorption onto ZIF-67.

	Pseudo-first order				Pseudo-second order		Weber-Morris model			
Initial Conc. (mg/L)	Qe, exp. (mg/g)	K_1 (min^{-1})	Qe, Cal (mg/g)	R^2	K_2 (g mg^{-1} min^{-1})	Qe, Cal (mg/g)	R^2	K_{int} (mg/g $min^{-0.5}$)	C (mg/g)	R^2
10	95.8	−0.0013	1.2316	0.9746	0.3454	99.20	0.9995	0.0504	0.0471	0.9525

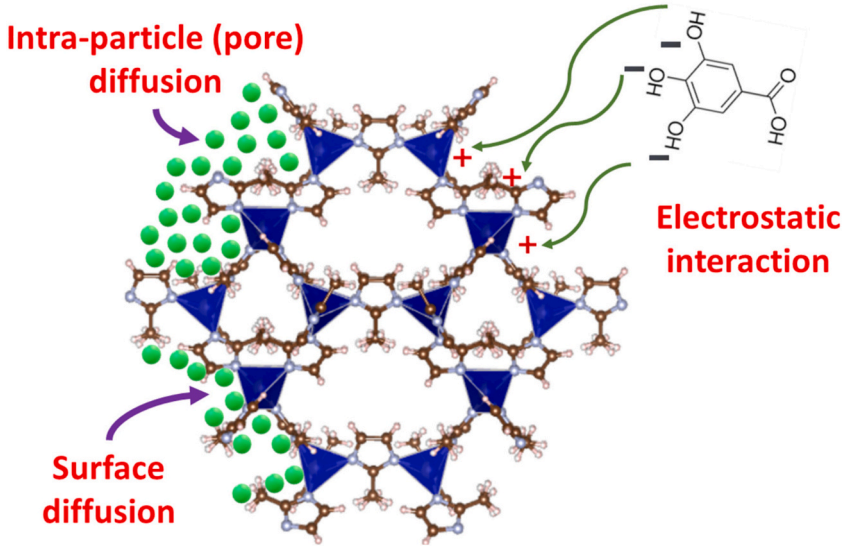

Fig. 11. Possible adsorption mechanism of GA onto ZIF-67.

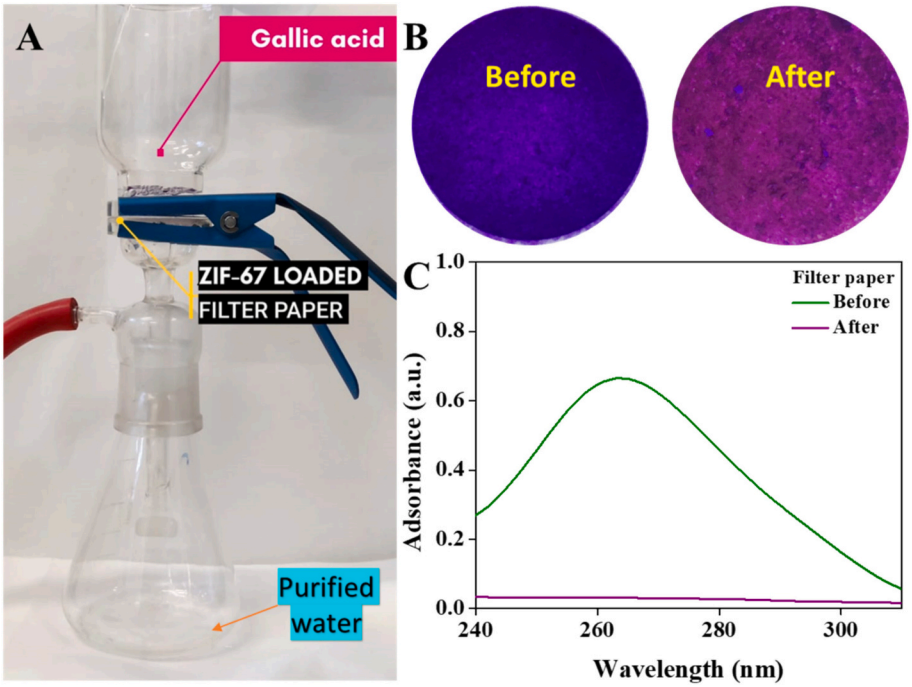

Fig. 12. (A) Demonstration of the removal of GA using the ZIF-67-based filter paper. (B) ZIF-67-based filter paper before and after GA adsorption. C) UV–vis GA solution before and after passage through the ZIF-67-based filter paper (initial C_{GA} = 10 mg/L; V = 100 mL).

and passed through the ZIF-67 filter in a continuous flow at 16.5 inHg with a flux of 983.86 L m^{-2} h^{-1}, as shown in video 1 and Fig. 12 A (more details are reported in the Supplementary Information file, S3).

The ZIF-67-modified filter paper exhibited an initial flux of 983.86 L m^{-2} h^{-1}, which remained stable over 0.5 h of continuous operation. The removal efficiency remained above 95% (confirmed by spectroscopic analysis (Fig. 12 C), indicating good operational stability and service life. The effectiveness of the GA adsorption on ZIF-67 was also visually evident from the colour change of the material after treatment (Fig. 12 B).

3.5. Heavy metals removal by ZIF@GA

Although the adsorption approach is a cost-effective way for water purification, it inevitably produces unwanted secondary waste in the form of exhausted adsorbents. The reuse of spent adsorbents offers a promising and economical solution to address disposal challenges while supporting environmental sustainability [73]. In this perspective, the spent ZIF-67, previously used for the GA abatement (ZIF@GA), was repurposed and evaluated for the removal of heavy metals from aqueous solutions. Pb(II) and Cd(II) were selected as representative cationic metals, whereas Cr(VI) was chosen as an anionic one.

In fact, depending on the solution pH value, hexavalent chromium (Cr(VI)) species in wastewater may be in different forms, such as chromate (CrO_4^{2-}), hydrogen chromate ($HCrO_4^-$), and dichromate ($Cr_2O_7^{2-}$). At neutral to alkaline pH (6.5–12), the dominant form of Cr(VI) is the more stable CrO_4^{2-} [74]. After the addition of ZIF@GA, the pH of the Cr (VI) mixture used for the adsorption tests reported in the present

manuscript was about 8.5. Therefore, CrO_4^{2-} was the main form of hexavalent chromium present in solution.

The corresponding adsorption results are presented in Fig. 13.

The adsorption efficiency of ZIF-67 towards Pb(II) removal is well documented in the literature [75,76]. Although the material's adsorption capability varies with the experimental conditions, in general this method remains time-consuming. In this regard, Fig. 13 A compares the adsorption performance of pristine ZIF-67 and ZIF@GA towards Pb(II) removal under identical conditions. As shown, ZIF@GA outperforms the pristine MOF, achieving a complete metal removal from the solution, whereas ZIF-67 removes about half. If on one hand the enhanced adsorption properties of ZIF@GA can be attributed to the GA modification of the MOF surface, acting as a chelating agent for metal cations [77], on the other hand it is worth assessing explicitly the effect of pH value on metals speciation and potential precipitation explicitly. Lead exists predominantly as Pb(II) in aqueous solution up to a pH value of approximately 6–7 [78]. At higher pH values, hydrolysed species, such as $Pb(OH)^+$, and less soluble forms, such as $Pb(OH)_2$, become increasingly prevalent. The latter, in particular, can precipitate under alkaline conditions, due to its low solubility.

To rule out the possibility that lead removal was due to precipitation rather than adsorption, the pH of the suspensions was measured before each of the two tests. In both cases, after the addition of the adsorbent the pH value was approximately 8.5. Under these conditions, lead is mainly present in solution as $Pb(OH)^+$, although the formation of the sparingly soluble $Pb(OH)_2$ precipitate cannot be entirely ruled out.

Despite the potential formation of minor precipitated lead species, the identical spontaneous pH values measured for both MOF suspensions permit to attribute the different Pb(II) removal efficiencies to the adsorbents themselves. The markedly superior adsorption properties of ZIF@GA can be associated to the presence of the polyphenol on the MOF surface, exploiting the carboxyl phenolic group on the surface of ZIF@GA able to coordinate metal cations [63], as confirmed by the FTIR spectrum of ZIF@GA@Pb showing a slight shift and intensity change of the the COO− bands, consistent with the participation of carboxylate/phenolic oxygen sites in Pb(II) binding (Fig. S12).

The effect of the initial Pb(II) concentration on the adsorption capacity of ZIF@GA was also investigated (Fig. 13 C). The results demonstrated that the material retained very promising activity up an initial Pb(II) concentration of 40 mg/L, after which ZIF@GA progressively achieves saturation of its active sites.

Moreover, the removal efficiency of Pb(II) over multiple adsorption cycles (five) is shown in Fig. 13 B. As it is possible to observe, the GA-modified MOF retained stable adsorption efficiency during the first two cycles, followed by a gradually decline over the subsequent three cycles, indicating a progressive saturation of the active sites on ZIF@GA and/or significant deterioration of the active adsorption sites. Even in this case, the structural evolution of the materials after five repeated Pb (II) adsorption cycles was properly evaluated (Fig. S13).

The characteristic Co—N stretching band (516 cm^{-1}) and imidazolate ring vibrations of C—N (1047 cm^{-1}) remain well evident in the FTIR spectrum of the spent material (Fig. S13 A), confirming partial retention of the coordination framework. Moreover, the characteristic signals of GA at 1506 cm^{-1} and 1366 cm^{-1}, referring to the symmetric and asymmetric stretching vibrations of the carboxylic O-C=O bonds, as well as the broad peak at 3369 cm^{-1} associated to the OH stretching, are still present. Finally, an additional peak at 612 cm^{-1}, assigned to the Pb—O bond, as a result of secondary adsorption, confirm the metal adsorption on the modified-MOF surface.

The XRD pattern (Fig. S13 B) of the spent material demonstrates a noticeable reduction in the intensity of ZIF-67 peaks, suggesting a partial loss of crystallinity. The decrease in peak intensity indicates a disruption

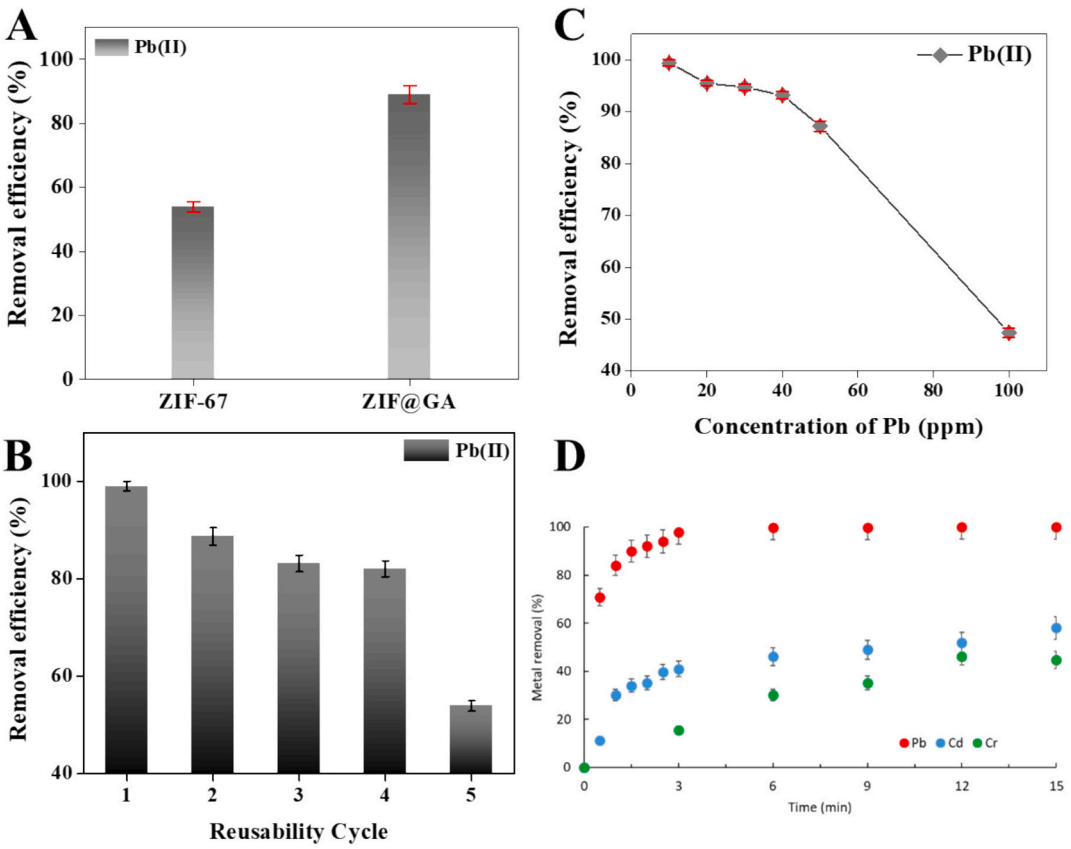

Fig. 13. A) Percentage of Pb(II) removal by pristine ZIF-67 and ZIF@GA (initial concentration of Pb(II) = 50 mg/L, adsorbent dose = 10 mg/L, contact time = 15 min); B) percentage of Pb(II) removal at various concentrations using ZIF-67@GA; C) reusability tests for Pb(II) removal by ZIF@GA; D) Percentage of metals (Pb(II), Cd(II), Cr(VI)) removal at various concentrations using ZIF-67@GA (10 mg/L), initial C_M = 10 mg/L.

of long-range order, likely due to the breaking of organic bonds or a change in the coordination environment of the metal.

As expected, at the end of Pb(II) adsorption, a pronounced reduction in the specific surface area (< 1 m^2/g (0.29 m^2/g)) was observed, as well as in the mean pore diameter (54 nm). This reduction is attributed to partial pore blockage by Pb(II) species and occupation of active sites, which explains the gradual decline in adsorption capacity beyond the fifth cycle. Such obstruction limits the availability of adsorption sites and mass transfer pathways, thereby accounting for the gradual decline in adsorption capacity observed beyond the fifth cycle. Even if the spent ZIF@GA@Pb seems to be characterized by a slight greater pore diameter value than spent ZIF@GA, at this very low value of surface are this discrepancy can be attributed to analytical uncertainty.

Additionally, leaching tests were conducted utilising ICP-OES analysis to ascertain the stability of ZIF-67, monitoring Co and Pb. Firstly, the leaching of Co ions from ZIF-67 was assessed after 1 h and 24 h of water contact, yielding leaching levels of 0.662 mg/L and 0.634 mg/L, respectively. The difference in the leaching between the two measurements (after 1 h and 24 h) was 0.028 mg/L, suggesting that the initial 1 h leaching level of cobalt ions (i.e., 0.662 mg/L) could be due to: (a) residual free cobalt ions which often remain unreacted during the synthesis of ZIF-67, (b) trapped precursors or byproducts retained due to unreacted ligands or solvents. According to the World Health Organisation (WHO), the suggested health-based value for cobalt in drinking water is 0.07 mg/L. Furthermore, the difference between 1 h and 24 h (i.e., 0.028 mg/L, which is less than 0.07 mg/L) indicates that only negligible amount of leaching of metal ions occurred during the contact time. In the case of ZIF@GA, the leaching test performed after lead adsorption displayed a metal release below the WHO guideline limit for lead in drinking water.

To assess the selectivity of ZIF@GA towards different metals ions, additional tests were performed for the removal of Cd(II) and Cr(VI). Fig. 13 D shows that ZIF-67@GA exhibited a different adsorption efficiency towards these additional metals compared to the results obtained for Pb(II). More in detail, while ZIF@GA exhibited a very high affinity towards Pb(II), achieving complete removal within only 3 min of contact time, its performance towards Cd(II) and Cr(VI) was noticeably lower. Under the same experimental conditions, removal efficiencies of 58% for Cd(II) and 45% for Cr(VI) were recorded after 15 min. The reduced affinity of ZIF@GA towards Cr(VI) species is easily attributed to electrostatic repulsion between the partially negative charges present on the surface of the MOF, due to the presence of GA, and the anionic metal in solution. Concerning Cd(II) abatement, precipitation of cadmium species occurs only at pH values above 10. Therefore, under the conditions employed here, Cd(II) removal is attributable solely to adsorption rather than precipitation.

Competitive adsorption analyses considering mixed metal ions systems were also performed to evaluate the selectivity mechanism of ZIF@GA towards Pb(II), Cd(II), and Cr(VI) uptake.

Fig. S14 displays that Pb(II) maintains the highest removal efficiency under competitive conditions, confirming its preferential adsorption behavior.

The observed selectivity can be explained by considering the solution chemistry at pH ≈ 8 and the surface functional groups of ZIF@GA. At this pH, a significant fraction of the –COOH groups from GA are deprotonated to $–COO^-$, providing negatively charged coordination sites. Both Pb(II) and Cd(II) can interact electrostatically with these sites; however, Pb(II) exhibits stronger complexation ability due to its higher polarizability and greater tendency to form inner-sphere complexes with oxygen-donor ligands ($–COO^-$, –OH).

In contrast, Cr(VI) predominantly exists as anionic species (CrO_4^{2-}) at pH 8, leading to electrostatic repulsion with the negatively charged surface sites and therefore significantly lower adsorption. Additionally, differences in hydrated ionic radius and hydrolysis behavior further contribute to the selectivity order observed: Pb(II) > Cd(II) > > Cr(VI). These combined electrostatic and coordination effects synergistically favor Pb(II) binding over competing ions in mixed systems.

3.5.1. Adsorption kinetics of Pb(II) over ZIF-67@GA

The adsorption kinetics were examined to ascertain the equilibrium time needed for the sorption of Pb(II) ions ZIF-67@GA. Since the efficiency of the adsorption process is closely linked to the contact time necessary to reach equilibrium, a time-dependent study was performed, as shown in Fig. 13 D. The results indicate that complete adsorption of Pb(II) occurs within 15 min. To further study the adsorption kinetics, the PFO and PSO reaction models were applied with the corresponding parameters summarised in Table 3.

As shown in Figs. S15 A and B, the PSO model provides a superior fit to the experimental data, reflected by an R^2 value approaching unity.

3.5.2. Adsorption isotherm

Further investigations were carried out to evaluate the adsorption behavior of Pb(II) onto ZIF-67@GA, as shown in Fig. S16 A and B and Table 4. The isotherm analysis shows that the Freundlich model provides a superior fit to the experimental data, with an R^2 value closer to unity compared to the Langmuir model. This indicates that Pb(II) adsorption onto ZIF-67@GA follows the Freundlich isotherm, consistent with a multilayer adsorption process occurring on a heterogeneous surface. Moreover, the maximum adsorption capacity ($q_{e,max}$) of ZIF-67@GA for Pb(II) was determined to be 1020 mg/g, highlighting the material's remarkable affinity for lead ions.

3.5.3. Comparison with other models

The adsorption performance of both ZIF-67 and ZIF-67@GA was compared with other adsorbents, as summarised in Tables S4 and S5.

When compared with recent data reported in the literature for GA removal from water matrices, ZIF-67 exhibits a very promising activity that outperforms that of common activated carbons, clays, agricultural waste-derived adsorbents, and other MOFs, as displayed in Table S4. ZIF-67 exhibits superior maximum adsorption capacity (171 mg/g) with a rapid equilibrium time of only 20 min at pH 5.

In contrast, most reported materials show significantly lower capacities (0.284–149 mg/g) and/or require much longer contact times (up to 7200 min). Importantly, ZIF-67 operates efficiently under mild, room-temperature conditions and maintains performance over 7 reusability cycles, demonstrating both kinetic and operational advantages.

Similarly, as reported in Table S5, ZIF-67@GA shows an exceptionally high adsorption capacity of 1020 mg/g towards Pb(II), compared to other materials. Moreover, adsorption equilibrium is achieved within only 15 min, highlighting both ultrafast kinetics and practical applicability. The material also retains performance over multiple reuse cycles (5 cycles).

Overall, these findings highlight ZIF-67 as a highly promising material for water purification applications. Its strong adsorption capabilities for both polyphenols and heavy metals, demonstrated by ZIF-67 and ZIF-67@GA, respectively, coupled with its rapid adsorption kinetics, underscore its potential utility in practical remediation processes. Moreover, the facile and sustainable synthesis of ZIF-67 supports the feasibility of industrial-scale production, while its low energy requirements further enhance its attractiveness for large-scale water treatment.

3.6. Complex mixture treatment by ZIF-67

Real water matrices contain a variety of complex components, such as humic substances, suspended solids, and co-existing organic and inorganic contaminants, which may significantly affect adsorption behavior of ZIF-67.

To systematically investigate the adsorption performance and interference resistance of the proposed material under simulated/real wastewater conditions, supplementary experiments were performed. In this regard, a series of additional experiments with progressively

Table 3
Kinetic parameters obtained from PFO and PSO models for ZIF-67@GA.

	Pseudo-first order				Pseudo-second order		
Initial Conc. (mg/L)	Qe, exp. (mg/g)	K_1 (min^{-1})	Qe, Cal (mg/g)	R^2	K_2 (g mg^{-1} min^{-1})	Qe, Cal (mg/g)	R^2
10	14.06	−0.0005	1.1984	0.1788	0.2325	19.31	0.9995

Table 4
Outline of Langmuir and the Freundlich isotherm parameters for ZIF-67@GA.

Langmuir isotherm			Freundlich isotherm		
K_L (L/mg)	R_L	R^2	1/n	K_F	R^2
37.01	0.0027	0.3022	1.87991	202.646	0.9215

increasing matrix complexity were realized.

First, competitive adsorption tests were conducted in deionized water using a binary system containing both GA and Pb(II) to investigate potential competition effects between the two main pollutants investigated in the present manuscript. More in detail, 10 mg of pristine ZIF-67 was dispersed in 20 mL of an aqueous solution containing both GA, (100 mg/L) and Pb(II) (10 mg/L). At the beginning, before the addition of the adsorbent, any potential interaction between the two pollutants was evaluated by UV–vis spectroscopy (Fig. S17). As it is possible to observe, no shift of the characteristic band of GA at 260 nm was observed, demonstrating the absence of any interaction between the two species present in solution. Subsequently, 10 mg of ZIF-67 was added to the previous mixture, and the mixture was maintained at room temperature under stirring for 30 min.

Then, the adsorbent was removed by filtration and the remaining residues of both GA and Pb(II) were analysed by UV–vis spectroscopy and atomic absorption spectroscopy, respectively.

The results, reported in Fig. 14 A, demonstrate that ZIF-67 simultaneously and effectively removed both the pollutants from the solution, confirming the fast adsorption capability of the investigated material.

Then, the complexity of the water matrix was improved. A simulated tap water matrix was prepared according to Annex B2 of the second protocol of the French Norm NF P41–650 [51], acidified by a few drops of nitric acid (0.4 M) until 5 pH value was achieved. Then, 2 mg of humic acid (HA) were added in 20 mL of simulated tap water, followed by 2 mg of GA (GA concentration in the final solution = 100 mg/L).

10 mg of ZIF-67 were added, and the mixture was maintained under stirring. After 15 min, the adsorbent was removed by filtration and the variation in concentration of GA was monitored by UV–vis spectroscopy. The results (97% of GA removal) confirmed the very promising adsorption properties of the investigated MOF. Finally, the complexity of the water matrix was enhanced, by the addition of Pb(II) (10 mg/L). Even under these conditions, ZIF-67 maintained its performance leading to the complete removal of both the species (92% GA, 99% Pb(II)), as shown in Fig. 14 B.

4. Conclusion

This work demonstrates the potential of ZIF-67 as an efficient and multifunctional adsorbent for advanced water purification. The material was successfully synthesised at room temperature and exhibited excellent adsorption performance towards polyphenolic contaminants, achieving up to 99% removal of gallic acid within minutes. Kinetic and isotherm analyses indicated that the adsorption process follows a pseudo-second-order model and is best described by the Freundlich isotherm, suggesting multilayer adsorption on heterogeneous active sites.A key novelty of this study lies in the development of a **sequential remediation strategy**, in which ZIF-67 is first employed for the rapid removal of polyphenols and subsequently reutilised for heavy-metal removal after adsorption of gallic acid. The resulting material (ZIF@GA) exhibited an exceptionally high adsorption capacity towards Pb(II) (1020 mg/g) and moderate removal efficiencies for Cd(II) and Cr (VI), demonstrating that the polyphenol-modified MOF surface can effectively act as a metal-binding platform. This approach introduces a **circular-economy concept**, transforming a spent adsorbent into a secondary functional material and significantly reducing secondary waste generation.

Another important innovation is the **immobilisation of ZIF-67 onto commercial filter paper**, which enabled efficient continuous-flow removal of gallic acid while maintaining high adsorption efficiency. This simple and scalable strategy overcomes the common limitations associated with powder MOFs, such as difficult recovery and handling, and provides a practical route towards real-time water treatment.

Overall, the combination of **rapid adsorption kinetics, sequential pollutant removal, and simple material immobilisation** highlights the practical relevance of ZIF-67-based systems for sustainable water remediation. The results demonstrate that this MOF platform can support **fast, flow-compatible and circular water purification**

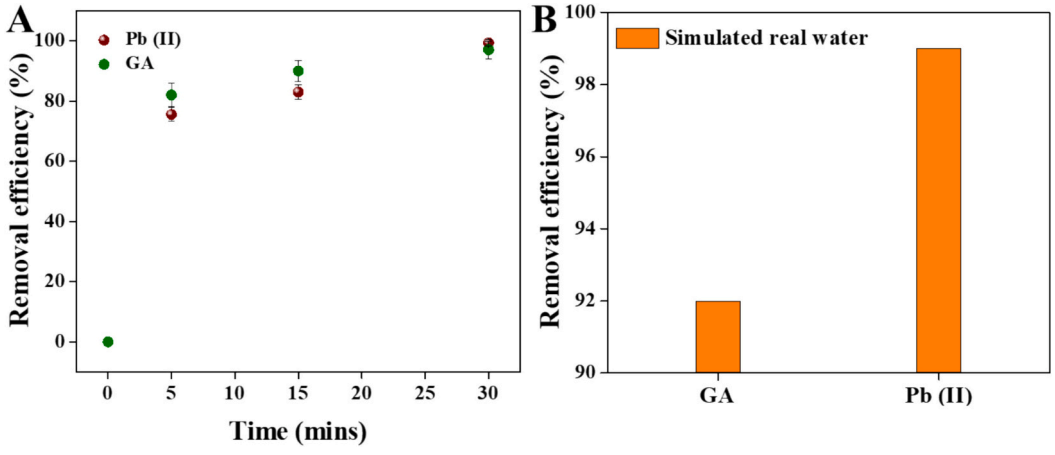

Fig. 14. Percentage of both GA and Pb(II) removal by ZIF-67 in deionized water (A) and simulated real water (B).

strategies, offering a promising pathway towards scalable and resource-efficient wastewater treatment technologies.

CRediT authorship contribution statement

Arvind Raj: Visualization, Methodology, Data curation, Conceptualization, Investigation, Formal analysis, Funding acquisition (MAECI), Writing – original draft. **Melissa G. Galloni:** Visualization, Investigation, Formal analysis. **Ermelinda Falletta:** Conceptualization, Resources, Supervision, Writing – review & editing. **Veronica Bortolotto:** Visualization, Investigation, Formal analysis. **Nikoletta Mila:** Investigation, Formal analysis. **Giuseppina Cerrato:** Data curation. **Valeria F. M. Mezzanotte:** Investigation, Formal analysis, Methodology, Data curation. **Mahaveer D. Kurkuri:** Supervision. **Claudia L. Bianchi:** Resources, Supervision.

Declaration of competing interest

The authors declare that they have no known competing financial interests or personal relationships that could have appeared to influence the work reported in this paper.

Acknowledgments

The financial support from the MAECI *Visiting* Fellowship, awarded by the Ministry of Foreign Affairs and International Cooperation (MAECI), Italian Government. This work was supported by Dipartimento di Chimica, Università degli Studi di Milano, Italy (Piano Sostegno alla Ricerca, PSR, grant 2023). We sincerely thank Jain University, Minor Project (JU/MRP/Univ/3/2022) for the financial support. TEM analyses were performed at the TEM facility of the Unitech COSPECT at the University of Milan (Italy). The authors thank Alessandro Perico for his contribution to the adsorption tests.

Appendix A. Supplementary data

Supplementary data to this article can be found online at https://doi.org/10.1016/j.seppur.2026.137783.

Data availability

Data will be made available on request.

References

[1] M. Abbas, F. Saeed, F.M. Anjum, M. Afzaal, T. Tufail, M.S. Bashir, A. Ishtiaq, S. Hussain, H.A.R. Suleria, Natural polyphenols: an overview, Int. J. Food Prop. 20 (2017) 1689–1699.
[2] G. Williamson, The role of polyphenols in modern nutrition, Nutr. Bull. 42 (2017) 226–235.
[3] H. Rasouli, M.H. Farzaei, R. Khodarahmi, Polyphenols and their benefits: a review, Int. J. Food Prop. 20 (2017) 1700–1741.
[4] A. Belščak-Cvitanović, K. Durgo, A. Huđek, V. Bačun-Družina, D. Komes, 1 - overview of polyphenols and their properties, in: C.M. Galanakis (Ed.), Polyphenols: Properties, Recovery, and Applications, Woodhead Publishing, 2018, pp. 3–44.
[5] A. Scalbert, I.T. Johnson, M. Saltmarsh, Polyphenols: antioxidants and beyond2, Am. J. Clin. Nutr. 81 (2005) 215S–217S.
[6] A. Ahmad, V. Ahmad, M.A. Zamzami, H. Chaudhary, O.A. Baothman, S. Hosawi, M. Kashif, M.S. Akhtar, M.J. Khan, Introduction and classification of natural polyphenols, in: S. Tabrez, M. Imran Khan (Eds.), Polyphenols-Based Nanotherapeutics for Cancer Management, Springer Singapore, Singapore, 2021, pp. 1–16.
[7] V. Hellwig, J. Gasser, Polyphenols from waste streams of food industry: valorisation of blanch water from marzipan production, Phytochem. Rev. 19 (2020) 1539–1546.
[8] Y. Wen, J. Wang, F. Wang, H. Wu, J. Zhou, Z. Dai, H. Guo, Recent advances in membranes modified with plant polyphenols in wastewater treatment: a review, Sep. Purif. Technol. 334 (2024) 125861.
[9] L. Bertin, F. Ferri, A. Scoma, L. Marchetti, F. Fava, Recovery of high added value natural polyphenols from actual olive mill wastewater through solid phase extraction, Chem. Eng. J. 171 (2011) 1287–1293.
[10] M. Salman, M.U. Farooq, A.U. Rahman, M. Yaseen, Polyphenols for wastewater and industrial influents treatment, in, Science and Engineering of Polyphenols (2024) 105–133.
[11] T. Deblonde, C. Cossu-Leguille, P. Hartemann, Emerging pollutants in wastewater: a review of the literature, Int. J. Hyg. Environ. Health 214 (2011) 442–448.
[12] R.L. Manasa, A. Mehta, Wastewater: Sources of pollutants and its remediation, in: K.M. Gothandam, S. Ranjan, N. Dasgupta, E. Lichtfouse (Eds.), Environmental Biotechnology Vol. vol. 2, Springer International Publishing, Cham, 2020, pp. 197–219.
[13] L. Li, J. Zhao, T. Yang, B. Sun, High-speed countercurrent chromatography as an efficient technique for large separation of plant polyphenols: a review, Food Res. Int. 153 (2022) 110956.
[14] M. Loginov, N. Boussetta, N. Lebovka, E. Vorobiev, Separation of polyphenols and proteins from flaxseed hull extracts by coagulation and ultrafiltration, J. Membr. Sci. 442 (2013) 177–186.
[15] P. Tapia-Quirós, M.F. Montenegro-Landívar, M. Reig, X. Vecino, J. Saurina, M. Granados, J.L. Cortina, Integration of membrane processes for the recovery and separation of polyphenols from winery and olive mill wastes using green solvent-based processing, J. Environ. Manag. 307 (2022) 114555.
[16] S. Todisco, P. Tallarico, B.B. Gupta, Mass transfer and polyphenols retention in the clarification of black tea with ceramic membranes, Innovative Food Sci. Emerg. Technol. 3 (2002) 255–262.
[17] A.J. Charlton, N.J. Baxter, M.L. Khan, A.J.G. Moir, E. Haslam, A.P. Davies, M. P. Williamson, Polyphenol/peptide binding and precipitation, J. Agric. Food Chem. 50 (2002) 1593–1601.
[18] P. Pérez-Larrán, B. Díaz-Reinoso, A. Moure, J.L. Alonso, H. Domínguez, Adsorption technologies to recover and concentrate food polyphenols, Curr. Opin. Food Sci. 23 (2018) 165–172.
[19] T.J. Buran, A.K. Sandhu, Z. Li, C.R. Rock, W.W. Yang, L. Gu, Adsorption/desorption characteristics and separation of anthocyanins and polyphenols from blueberries using macroporous adsorbent resins, J. Food Eng. 128 (2014) 167–173.
[20] L. Sun, Y. Guo, C. Fu, J. Li, Z. Li, Simultaneous separation and purification of total polyphenols, chlorogenic acid and phlorizin from thinned young apples, Food Chem. 136 (2013) 1022–1029.
[21] X. Pan, J. Ji, N. Zhang, M. Xing, Research progress of graphene-based nanomaterials for the environmental remediation, Chin. Chem. Lett. 31 (2020) 1462–1473.
[22] Z.P. Gao, Z.F. Yu, T.L. Yue, S.Y. Quek, Adsorption isotherm, thermodynamics and kinetics studies of polyphenols separation from kiwifruit juice using adsorbent resin, J. Food Eng. 116 (2013) 195–201.
[23] Y. Ma, X. Liu, X. Xu, M. Wu, J. Sun, N. Niu, L. Chen, A compressible and underwater superelastic hydrophilic molecularly imprinted resin composite cellulose nanofiber aerogel to separate and purify catechins from tea, Chem. Eng. J. 472 (2023) 145043.
[24] Z. Sun, Y. Liao, Y. Zhang, S. Sun, Q. Kan, Z. Wu, L. Yu, Z. Dong, Z. Wang, R. He, L. Wang, Q. Meng, H. Wang, Q. Wang, L. Mao, D. Pan, S. Wang, Z. Zhang, W. Zhu, S. Liu, M. Wakeel, B. Hu, T. Duan, X. Tai, X. Wang, Sustainable carbon materials in environmental and energy applications, Sustainable Carbon Materials 1 (2025) e007.
[25] A. Mir-Cerdà, V. Ramos-Calero, J.L. Beltrán, J.L. Cortina, J. Saurina, S. Sentellas, M. Granados, Towards a sustainable recovery of polyphenols from agrifood waste: performance of polymeric sorbents with natural deep eutectic solvent extracts, LWT 207 (2024) 116632.
[26] P.V. Mane, R.M. Rego, P.L. Yap, D. Losic, M.D. Kurkuri, Unveiling cutting-edge advances in high surface area porous materials for the efficient removal of toxic metal ions from water, Prog. Mater. Sci. 146 (2024) 101314.
[27] M.G. Galloni, V. Nikonova, G. Cerrato, A. Giordana, P. Pleva, P. Humpolicek, E. Falletta, C.L. Bianchi, Novel eco-friendly and easily recoverable bismuth-based materials for capturing and removing polyphenols from water, J. Environ. Manag. 369 (2024) 122365.
[28] R.M. Rego, G. Kuriya, M.D. Kurkuri, M. Kigga, MOF based engineered materials in water remediation: recent trends, J. Hazard. Mater. 403 (2021) 123605.
[29] R.M. Rego, M.D. Kurkuri, M. Kigga, A comprehensive review on water remediation using UiO-66 MOFs and their derivatives, Chemosphere 302 (2022) 134845.
[30] A. Raj, R.M. Rego, K.V. Ajeya, H.-Y. Jung, M.D. Kurkuri, Basil seeds loaded with MOFs as an eco-friendly and sustainable adsorbent for efficient removal of hazardous organic pollutants from water, Sep. Purif. Technol. 330 (2024) 125370.
[31] M. Mon, R. Bruno, J. Ferrando-Soria, D. Armentano, E. Pardo, Metal–organic framework technologies for water remediation: towards a sustainable ecosystem, J. Mater. Chem. A 6 (2018) 4912–4947.
[32] P. Samanta, A.V. Desai, S. Let, S.K. Ghosh, Advanced porous materials for sensing, capture and detoxification of organic pollutants toward water remediation, ACS Sustain. Chem. Eng. 7 (2019) 7456–7478.
[33] S.J.C.S.R. Kitagawa, Metal–organic frameworks (MOFs), Chem. Soc. Rev. 43 (2014) 5415–5418.
[34] S.L. James, Metal-organic frameworks, Chem. Soc. Rev. 32 (2003) 276–288.
[35] Introduction to Metal–Organic Frameworks, Chem. Rev. 112 (2012) 673–674.
[36] K.K. Gangu, S. Maddila, S.B. Mukkamala, S.B. Jonnalagadda, A review on contemporary Metal–Organic Framework materials, Inorg. Chim. Acta 446 (2016) 61–74.
[37] S. Wang, C.M. McGuirk, A. d'Aquino, J.A. Mason, C.A. Mirkin, Metal–Organic Framework Nanoparticles 30 (2018) 1800202.
[38] A. Raj, R.M. Rego, K.V. Ajeya, H.-Y. Jung, T. Altalhi, G.M. Neelgund, M. Kigga, M. D. Kurkuri, Underwater oleophobic-super hydrophilic strontium-MOF for efficient oil/water separation, Chem. Eng. J. 453 (2023) 139757.

[39] R.M. Rego, G. Sriram, K.V. Ajeya, H.-Y. Jung, M.D. Kurkuri, M. Kigga, Cerium based UiO-66 MOF as a multipollutant adsorbent for universal water purification, J. Hazard. Mater. 416 (2021) 125941.
[40] C.S. Dzah, Y. Duan, H. Zhang, N.A. Serwah Boateng, H. Ma, Latest developments in polyphenol recovery and purification from plant by-products: a review, Trends Food Sci. Technol. 99 (2020) 375–388.
[41] H. Furukawa, K.E. Cordova, M. O'Keeffe, O.M. Yaghi, The Chemistry and Applications of Metal-Organic Frameworks, Science 341 (2013) 1230444.
[42] S. Şahin, E. Abdelillah Ali Elhussein, M. Abdel Salam, Ş.S. Bayazit, Recovery of polyphenols from water using zr-based metal-organic frameworks and their nanocomposites with graphene nanoplatelets, J. Ind. Eng. Chem. 78 (2019) 164–171.
[43] A.R. Bagheri, M. Ghaedi, Application of cu-based metal-organic framework (cu-BDC) as a sorbent for dispersive solid-phase extraction of gallic acid from orange juice samples using HPLC-UV method, Arab. J. Chem. 13 (2020) 5218–5228.
[44] N. Kahkeshani, F. Farzaei, M. Fotouhi, S.S. Alavi, R. Bahramsoltani, R. Naseri, S. Momtaz, Z. Abbasabadi, R. Rahimi, M.H. Farzaei, A. Bishayee, Pharmacological effects of gallic acid in health and diseases: a mechanistic review, Iran. J. Basic Med. Sci. 22 (2019) 225–237.
[45] G. Zhong, D. Liu, J. Zhang, The application of ZIF-67 and its derivatives: adsorption, separation, electrochemistry and catalysts, J. Mater. Chem. A 6 (2018) 1887–1899.
[46] H.U. Escobar-Hernandez, Y. Quan, M.I. Papadaki, Q. Wang, Life Cycle Assessment of Metal–Organic Frameworks: Sustainability Study of Zeolitic Imidazolate Framework-67, ACS Sustain. Chem. Eng. 11 (2023) 4219–4225.
[47] X. Qian, Q. Ren, X. Wu, J. Sun, H. Wu, J. Lei, Enhanced Water Stability in Zn-Doped Zeolitic Imidazolate Framework-67 (ZIF-67) for CO2 Capture Applications, Chemistry Select 3 (2018) 657–661.
[48] A. Bendre, V. Hegde, K.V. Ajeya, S. Thagare Manjunatha, D. Somasekhara, V. K. Nadumane, K. Kant, H.-Y. Jung, W.-S. Hung, M.D. Kurkuri, Microfluidic-assisted synthesis of metal—organic framework —alginate Micro-particles for sustained, Drug Deliv. 13 (2023) 737.
[49] V. Acevedo-García, E. Rosales, A. Puga, M. Pazos, M.J.S. Sanromán, P. Technology, Synthesis and use of efficient adsorbents under the principles of circular economy: Waste valorisation and electroadvanced oxidation process regeneration 242 (2020) 116796.
[50] R.M. Rego, K.V. Ajeya, H.-Y. Jung, S. Kabiri, M. Jafarian, M.D. Kurkuri, M. Kigga, Nanoarchitectonics of Bimetallic MOF@Lab-Grade Flexible Filter Papers: An Approach Towards Real-Time Water Decontamination and Circular Economy vol. 19, 2023, p. 2302692.
[51] L. Rimoldi, D. Meroni, E. Falletta, V. Pifferi, L. Falciola, G. Cappelletti, S. Ardizzone, Emerging pollutant mixture mineralization by TiO2 photocatalysts, The role of the water medium, Photochemical & Photobiological Sciences 16 (2017) 60–66.
[52] Q. Jiang, N. Chai, T. Liu, S. Ying, Y. Kong, T. Chen, Q. Guo, F.-Y. Yi, Investigating and improving the water stability of ZIF-L-co for electrochemical glucose sensors, Microchem. J. 201 (2024) 110538.
[53] S.A. Ahmed, D. Bagchi, H.A. Katouah, M.N. Hasan, H.M. Altass, S.K. Pal, Enhanced water stability and photoresponsivity in metal-organic framework (MOF): a potential tool to combat drug-resistant bacteria, Sci. Rep. 9 (2019) 19372.
[54] S. Zheng, Y. Xu, X. Yao, C. Wang, P. Liu, H. Zhao, J. Lu, J. Ju, Efficient Removal of Tetracycline by Metal–Organic Framework ZIF-67 and Its Mechanism, Separations 11 (2) (2024) 63.
[55] K.-Y.A. Lin, H.-A. Chang, Ultra-high adsorption capacity of zeolitic imidazole framework-67 (ZIF-67) for removal of malachite green from water, Chemosphere 139 (2015) 624–631.
[56] M.A. Nazir, S. Ullah, M.U. Shahid, I. Hossain, T. Najam, M.A. Ismail, A.U. Rehman, M.R. Karim, S.S.A. Shah, Zeolitic Imidazolate Frameworks (ZIF-8 & ZIF-67): Synthesis and Application for Wastewater Treatment, Sep. Purif. Technol. vol. 356 (2025) 129828.
[57] J. Xiao, Recent advances on the stability of dietary polyphenols, eFood 3 (3) (2022) e21.
[58] N. Talukder, Y. Wang, B.B. Nunna, X. Tong, E.S. Lee, An investigation on the structural stability of ZIF-8 in water versus water-derived oxidative species in aqueous environment, Microporous Mesoporous Mater. 366 (2024) 112934.
[59] J. Cai, L. Jiang, H. Wei, C. Wang, L. Yu, L. Zhang, Preparation of carbon/cobalt composite from phenolic resin and ZIF-67 for efficient tannic acid adsorption, Microporous Mesoporous Mater. 287 (2019) 9–17.
[60] Y. Pan, Z. Li, Z. Zhang, X.-S. Tong, H. Li, C.-Z. Jia, B. Liu, C.-Y. Sun, L.-Y. Yang, G.-J. Chen, D.-Y. Ma, Adsorptive removal of phenol from aqueous solution with zeolitic imidazolate framework-67, J. Environ. Manag. 169 (2016) 167–173.
[61] K.M. Ansy, J.-H. Lee, H. Piao, G. Choi, J.-H. Choy, Stabilization of antioxidant gallate in layered double hydroxide by exfoliation and reassembling reaction, Solid State Sci. 80 (2018) 65–71.
[62] N.T. Thanh Tu, T.V. Thien, P.D. Du, V.T. Thanh Chau, T.X. Mau, D.Q. Khieu, Adsorptive removal of Congo red from aqueous solution using zeolitic imidazolate framework–67, journal of environmental, Chem. Eng. 6 (2018) 2269–2280.
[63] Y. Li, K. Zhou, M. He, J. Yao, Synthesis of ZIF-8 and ZIF-67 using mixed-base and their dye adsorption, Microporous Mesoporous Mater. 234 (2016) 287–292.
[64] E. Rápó, S. Tonk, Factors affecting synthetic dye adsorption, Desorption Studies: A Review of Results from the Last Five Years 26 (2021) (2017–2021) 5419.
[65] H.-K. Chung, W.-H. Kim, J. Park, J. Cho, T.-Y. Jeong, P.-K. Park, Application of Langmuir and Freundlich isotherms to predict adsorbate removal efficiency or required amount of adsorbent, J. Ind. Eng. Chem. 28 (2015) 241–246.
[66] P.K. Chattaraj, H. Lee, R.G. Parr, HSAB principle, J. Am. Chem. Soc. 113 (1991) 1855–1856.
[67] X. Liu, Y. Shan, S. Zhang, Q. Kong, H. Pang, Application of metal organic framework in wastewater treatment, green, Energy Environ. 8 (2023) 698–721.
[68] G. Shi, C. Ruan, S. He, H. Pan, G. Chen, Y. Ma, H. Dai, X. Chen, X. Yang, Zr-based MOF @ carboxymethylated filter paper: insight into construction and methylene blue removal mechanism, Colloids Surf. A Physicochem. Eng. Asp. 613 (2021) 126053.
[69] C. Yang, J. Wang, W. Yan, Y. Xia, Facile synthesis disposable MOF membrane filter: growth of NH2-MIL-125 (ti) on filter paper for fast removal of organophosphorus pesticides in aqueous solution and vegetables, Food Chem. 389 (2022) 133056.
[70] Z. Cai, Y. Luo, L. Gan, ZIF-67(Co)-Loaded Filter Paper for In Situ Catalytic Degradation of Bisphenol A in Water, Separations 9 (11) (2022) 340.
[71] H.N. Abdelhamid, A.P. Mathew, In-situ growth of zeolitic imidazolate frameworks into a cellulosic filter paper for the reduction of 4-nitrophenol, Carbohydr. Polym. 274 (2021) 118657.
[72] J. Park, M. Oh, Construction of flexible metal–organic framework (MOF) papers through MOF growth on filter paper and their selective dye capture, Nanoscale 9 (2017) 12850–12854.
[73] B.G. Fouda-Mbanga, O.P. Onotu, Z. Tywabi-Ngeva, Advantages of the reuse of spent adsorbents and potential applications in environmental remediation: a review, Green Anal. Chem. 11 (2024) 100156.
[74] M. Ao, R. Zhou, R. Meng, L.A. Bonaventure, B. Luo, X. Qian, X. Xu, S. Wang, P. Wu, Chromium transformations and biological impacts in aquatic systems: from sediment-water interfaces to food web complexity, Ecotoxicol. Environ. Saf. 303 (2025) 118850.
[75] K. Ahmad, H.-U.-R. Shah, M.S. Khan, A. Iqbal, E. Potrich, L.S. Amaral, S. Rasheed, H. Nawaz, A. Ayub, K. Naseem, A. Muhammad, M.R. Yaqoob, M. Ashfaq, Lead in drinking water: adsorption method and role of zeolitic imidazolate frameworks for its remediation: a review, J. Clean. Prod. 368 (2022) 133010.
[76] F. Zadehahmadi, N.T. Eden, H. Mahdavi, K. Konstas, J.I. Mardel, M. Shaibani, P. C. Banerjee, M.R. Hill, Removal of metals from water using MOF-based composite adsorbents, Environ. Sci.: Water Res. Technol. 9 (2023) 1305–1330.
[77] H. Qiu, W. Ni, L. Yang, Q. Zhang, Remarkable ability of Pb(II) capture from water by self-assembled metal-phenolic networks prepared with tannic acid and ferric ions, Chem. Eng. J. 450 (2022) 138161.
[78] A.D. Davis, C.J. Webb, J.L. Sorensen, D.J. Dixon, R. Hudson, Geochemical thermodynamics of lead removal from water with limestone, Water Air Soil Pollut. 229 (2018) 177.